THE EFFECTS OF BANDWIDTH REDUCTION ON CROSS-CORRELATION COMPUTATIONS IN THE ANALYSES OF RECORDED GUNSHOT SOUNDS

by

DOUGLAS SCOTT LACEY

B.S., University of Miami, 1996

A thesis submitted to the

Faculty of the Graduate School of the

University of Colorado in partial fulfillment

of the requirements for the degree of

Master of Science

Recording Arts Program

2019

This thesis for the Master of Science degree by

Douglas Scott Lacey

has been approved for the

Recording Arts Program

by

Catalin Grigoras, Chair

Jeffrey M. Smith

Robert C. Maher

Date: December 14, 2019

Lacey, Douglas Scott (M.S., Recording Arts Program)

The Effects of Bandwidth Reduction on Cross-Correlation Computations in the Analyses of Recorded Gunshot Sounds

Thesis directed by Associate Professor Catalin Grigoras

ABSTRACT

Forensic audio examiners often use quantitative measures, such as cross-correlation computations, of recorded gunshot sounds in an attempt to assess the number of different firearms that were fired and to determine which gunshot events are consistent with having been fired by the same firearm. When used in conjunction with ballistics evidence gathered at the scene, conclusions drawn from such analyses can assist in establishing a timeline of events and answer questions such as "who fired first?" Forensic recordings are typically made in uncontrolled environments and are of low quality compared to recordings made in controlled environments (such as recording studios) using high-quality microphones and uncompressed audio formats with high sampling rates and wide dynamic range. The relatively poor quality, limited bandwidth, and lossy compression artifacts in forensic recordings, combined with uncontrolled acoustic conditions, can negatively affect the reliability of quantitative analyses. This thesis examines the effects of bandwidth reduction on cross-correlation computations of recorded gunshot sounds captured in a controlled environment with a high-quality recording system.

The form and content of this abstract are approved. I recommend its publication.

Approved: Catalin Grigoras

I dedicate this thesis to my wife, Holly Breault, who continually motivates and supports me in my professional endeavors and my personal life. I owe my Beautiful an unrepayable debt of gratitude for making me strive for greater things. 143.

And to my mom, Donna Lacey, who along with my late dad, Richard Lacey, provided a nurturing environment which enabled me to pursue my educational and career goals, and who patiently stuck with me when those goals changed over time.

ACKNOWLEDGEMENTS

I would like to thank Dr. Robert C. Maher for his ongoing and highly informative research into gunshot acoustics and analysis. Of particular importance to this thesis is his U.S. Department of Justice-funded research project titled “Advancing Audio Forensics of Gunshot Acoustics.” The database of gunshot recordings utilized in this thesis was produced by Dr. Maher and his team as part of this research project and was kindly made available publicly through the Office of Justice Programs’ National Criminal Justice Reference Service.

I am also indebted to my mentor, colleague, and friend Bruce Koenig, for his guidance and professional partnership over the past 23 years. When approaching complicated problems, he encouraged me to think more like a scientist and less like an engineer. In the words of (Dirty) Harry Callahan, “A man's got to know his limitations.”

Steve Beck also receives my sincere thanks for letting me bend his ear on a number of occasions regarding his research into recorded gunshot analysis and for his continuing interest and ongoing research in the field.

Lastly, I would be remiss if I didn’t thank Dr. Catalin Grigoras, Jeff Smith, Cole Whitecotton, and Leah Haloin at the University of Colorado Denver, for their encouragement throughout the Master’s program and their tireless efforts with keeping the program (and students) running smoothly. Cole receives special recognition for running massive amounts of computational data for me in the 11th hour.

TABLE OF CONTENTS

CHAPTER

LIST OF TABLES

TABLE

LIST OF FIGURES

FIGURE

INTRODUCTION

Gunshot Analysis

The forensic analysis of recorded gunshot sounds, while requested less frequently than audio enhancement and audio authentication, can provide critical information during an investigation of criminal activity or of actions related to civil litigation. With the proliferation of mobile devices and law enforcement body cameras, and the widespread adoption of home and business video surveillance systems, the likelihood that gunshots occurring in urban and rural environments will be recorded has increased. And with that increase comes greater opportunity for analysis.

Requests for recorded gunshot analysis typically center on one (1) or more of the following questions [1]:

- Are these sounds gunshots?
- How many gunshots were there?
- How many firearms were there?
- How many and which gunshots did each firearm discharge?
- Who fired first?
- What are the firearm types/calibers?
- Where was each shooter positioned?
- What is the timing between gunshots?

Various techniques may be employed to analyze the recorded audio and to draw conclusions to address the questions posed above. These techniques may include pre-processing/filtering of signals, critical listening, time-domain (waveform) analysis, energy/envelope analysis, frequency-domain analysis, cross-correlation computations, and time difference of arrival (TDOA) [1]. The focus of the present research and thesis is on the use of cross-correlation computations in the analysis of recorded gunshot sounds and does not directly address the other listed techniques.

Prior Research

Gunshot Acoustics

The mechanisms of firearms and the acoustical characteristics of their discharges have been covered by several research papers and presentations aimed at the audio forensics and signal processing fields. Many of these papers/presentations have resulted from the work of Dr. Robert C. Maher (Montana State University, Department of Electrical and Computer Engineering) and his colleagues.

Maher and Shaw [2-4] have previously discussed the principle mechanics of a gunshot and placed these elements in context with the acoustical signals which are produced by the event. They also identified limitations of capturing gunshots in “real world” conditions with less-than-ideal microphone and recording systems.

Figure 1 provides an acoustical, time-domain overview of a .308 caliber rifle firing a supersonic bullet (i.e., faster than the speed of sound) and recorded by two (2) professional-quality microphones at different locations in a controlled environment [4]. The supersonic bullet produces a shock wave which is followed by its ground reflection, both of which arrive at the microphones prior to the muzzle blast, which is traveling at the speed of sound. A ground reflection of the muzzle blast then ends the sequence. In the case of a bullet traveling at less than the speed of sound, no shock wave (or reflected shock wave) would be present.

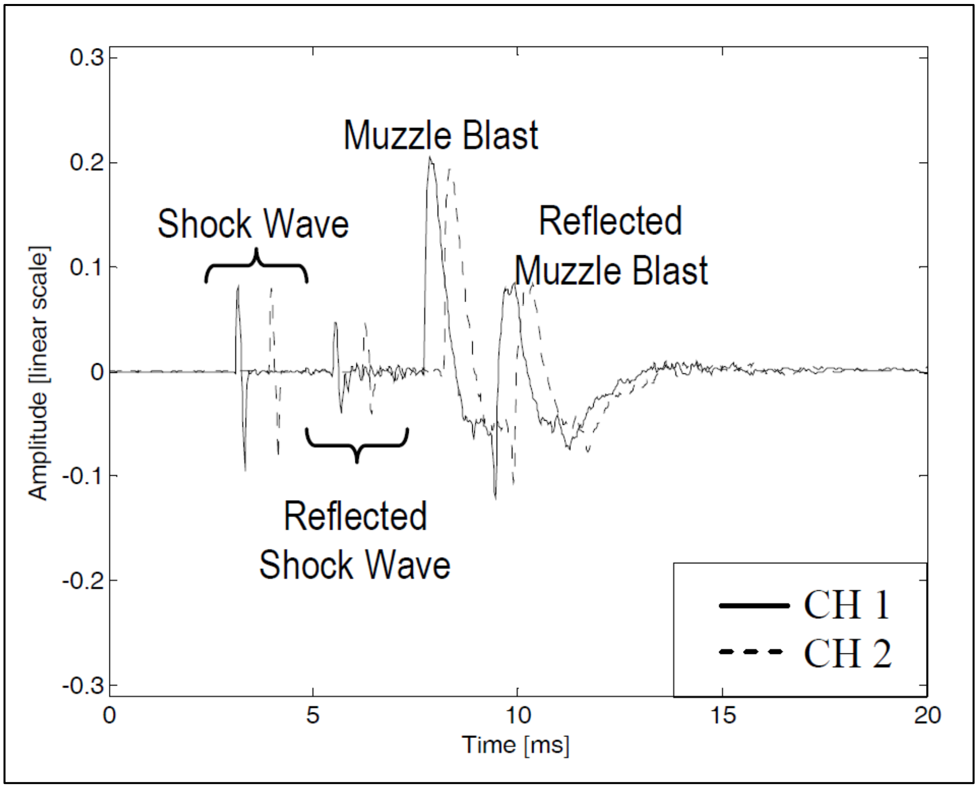

Figure 1 – Time-aligned waveforms for a 2-channel recording of a supersonic bullet fired from a .308 caliber rifle, illustrating the basic acoustical elements of the gunshot [4].

The shock wave expands in a conical fashion behind the bullet, and the angle at which the shock wave front propagates is relative to the bullet's speed divided by the speed of sound, a value referred to as the Mach Number [2, 3]. The higher the Mach Number, the shallower the angle of the shock wave front is relative to the bullet's trajectory, as depicted in Figure 2 [4]. As the shock wave passes the microphone diaphragm, it causes a positive overpressure maximum followed by a corresponding under-pressure minimum, which forms an "N" shape in the waveform; this "N" shape can be seen in the Figure 1 waveforms and is provided in more detail in Figure 3 [2].

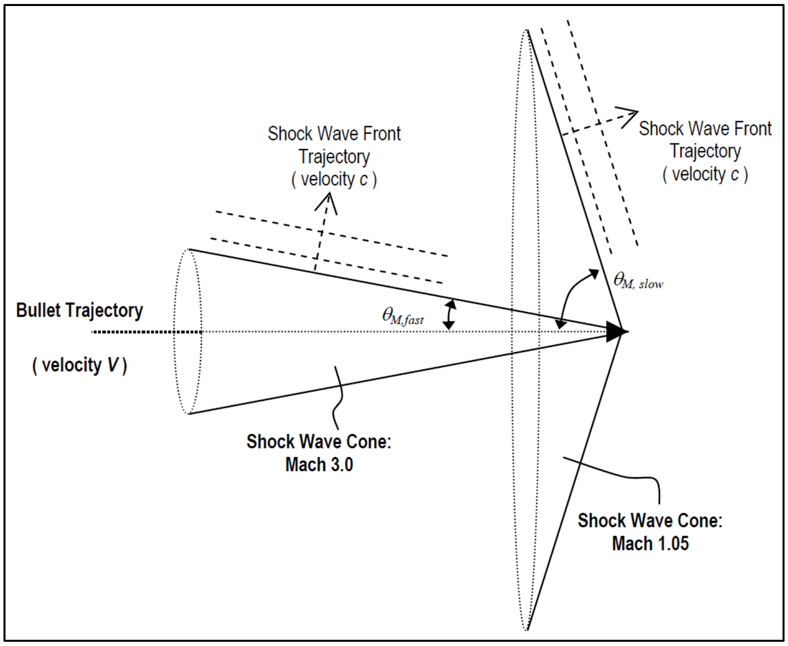

Figure 2 – Comparisons of the shock wave geometry for a bullet traveling at Mach 1.05 and Mach 3 [4].

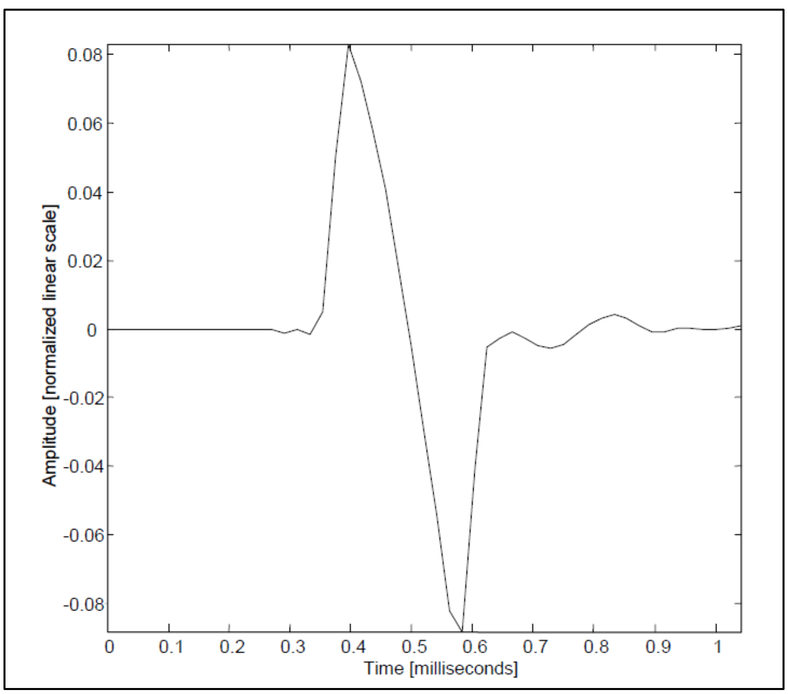

Figure 3 – Detail of a recording of an "N" wave caused by a supersonic bullet passing the diaphragm of a microphone [2].

Cross-Correlation Computations

Cross-correlation computations provide for a quantitative measure indicating the similarity between two (2) signals and is defined by the following equation [5, 6]:

$$\hat{R}_{xy}(m) = \begin{cases} \displaystyle\sum_{n=0}^{N-m-1} x_{n+m} y_n^* & m \geq 0 \\ \hat{R}_{yx}^*(-m) & m < 0 \end{cases} \tag{1}$$

In equation (1), "*x*" and "*y*" refer to the input signals of sample length "*N*", and "*m*" is the displacement (or lag) in samples as "*x*" and "*y*" are slid over each other while the cross-correlation computations are performed. Normalization of the output, such that the cross-correlation value computed of a signal aligned sample-for-sample with itself (i.e., autocorrelation) will be +1, is achieved by dividing the output of equation (1) by the product of the norms of "*x*" and "*y*", as follows [5, 6]:

$$Normalized\ \hat{R}_{xy}(m) = \frac{\hat{R}_{xy}(m)}{\left(\sqrt{x_1^2 + x_2^2 + \cdots + x_N^2}\right)\left(\sqrt{y_1^2 + y_2^2 + \cdots + y_N^2}\right)} \tag{2}$$

The resulting normalized cross-correlation values will be constrained between –1 and +1, with +1 being the autocorrelation result (as indicated above) and –1 being the autocorrelation result with one (1) of the signals being 180° out of phase. The normalized cross-correlation value will approach 0 for two (2) signals that are completely uncorrelated (e.g., true white noise).

Koenig et al. [7] explored the application of cross-correlation computations to the forensic analysis of recorded gunshot sounds through a collection of gunshots fired on an outdoor firing range by five (5) firearms at four (4) different positions, relative to the locations of nine (9) recording/sensing devices which simultaneously recorded the shots. The recording/sensing devices ranged from consumer- to professional-grade and included law enforcement-specific devices. Nearly all the recording/sensing systems were analog, and all were commonly encountered by forensic audio examiners at the time that the research was conducted. Cross-correlation computations were run, in part, for shots from the same firearm ("cross shot"), and were compared with visual, qualitative assessments of the corresponding waveforms. The general hierarchy given in Table 1 summarizes the correspondence of the qualitative, visual observations of the waveforms with the quantitative cross-correlation results for the "cross shot" events.

Table 1 – Summary of the qualitative and quantitative results from [7].

Visual Observation	Average Correlation	Correlation Range
Excellent	0.920	0.645-0.997
Good	0.834	0.610-0.976
Fair	0.686	0.364-0.942
Poor	0.498	0.253-0.692

As an extension to the research conducted by Koenig, et al. [7], a new set of gunshots was recorded using digital audio recorders [16-bit pulse code modulation (PCM) encoding; 96,000 samples per second or 96 kilohertz (kHz)] and four (4) B&K model 4136 microphones with wide frequency response (flat from 4 Hz to 70 kHz) and dynamic range [greater than 172 decibels (dB)]. The microphones were arranged in six (6) different configurations of distance and angle, relative to the position of the firearm, as given in Table 2 [8].

Table 2 – Firearm-to-microphone distances (Range) and azimuth angles relative to the line of fire for the six (6) firearm recording configurations [8].

Configuration	Range (m)	Azimuth angle (deg)
1	1.5, 3, 6, 30	3
2	1.5, 3, 6, 30	90
3	3	3, 30, 60, 90
4	30	3, 30, 60, 90
5	3	90, 120, 150, 180
6	30	90, 120, 150, 180

Seven (7) different firearms were utilized in [8], some firing multiple types of ammunition, and cross-correlation computations arrived at similar results to [7]. Namely, "successive-shot correlations with source, environment, and receiver variations held constant are very high", and "[c]orrelations between waveforms from different angles and different distances are typically lower than those between successive shots."

Limitations

An overriding observation that pervades much of the prior research conducted in the field of recorded gunshot analysis is that there are many factors that affect the ability to answer the common questions listed above and to otherwise draw meaningful conclusions. These factors include, but are not limited to, the following [7-9]:

- Microphone type
- Distance between the microphone and the firearm
- Relative angle between the microphone and firearm
- Recorder settings
- Acoustical environment
- Type of firearm discharged

- Differences in ammunition
- Muzzle blast size

Because these factors affect how a gunshot is ultimately recorded, they also impact the quantitative results that are derived from those recordings.

Research Focus

While many factors come into play when analyzing recorded gunshot sounds, such as those listed above, this thesis focuses on how reductions in the audio bandwidth affect the quantitative results arrived at through the application of cross-correlation. In real-world cases, the forensic examiner does not typically have the benefit of receiving high-quality, controlled recordings, nor multiple simultaneous recordings of the same series of events. The utilization of a controlled database of gunshot recordings for this thesis (discussed below in the "MATERIALS" chapter) allowed for wide flexibility regarding the production of reduced bandwidth recordings of the same gunshot event, thereby permitting observations to be made of cross-correlation computations as the bandwidth is reduced.

With the reduction of the recorded bandwidth comes the removal of high-frequency components within the recorded gunshots, which is expected to lead to fewer distinctive features between intra- and inter-firearm gunshots (i.e., the recorded gunshot sounds will appear more alike as the bandwidth is reduced). Accordingly, the central hypotheses that were tested for this thesis are as follows:

- As the bandwidth of an audio recording is decreased, the corresponding cross-correlation results for <u>intra</u>-firearm comparisons will increase.

- As the bandwidth of an audio recording is decreased, the corresponding cross-correlation results for inter-firearm comparisons will increase.
- The ability to statistically distinguish between recorded gunshot sounds from different firearms may be compromised as the bandwidth of an audio recording is decreased.

MATERIALS

Recorded Gunshot Database

The recorded gunshot database that arose from Maher and Routh [10, 11], and subsequently made publicly available on-line [12], was used as the basis for the research conducted for this thesis. This database was collected anechoically (i.e., without early sound reflections) in an outdoor environment in Montana, USA, and under conditions which were designed to be scientifically reliable and repeatable. The creation of this database was unique in several ways, as discussed below, and provided recorded data that was tailor-made for exploring the effect of frequency bandwidth reduction (through downsampling) on cross-correlation computations.

Firearms and Shots

Table 3 provides a listing of the ten (10) firearm/caliber scenarios that were used during the database collection process, with two (2) different calibers of ammunition (.38 and .357) fired by the Ruger SP101 handgun.

Table 3 – Firearm and shot information [11, 12].

Scenario	Firearm	Caliber	# of Shots
1	Glock 23 handgun	.40	10
2	Glock 19 handgun	9mm	10
3	SIG Sauer P239 handgun	.357	10
4	Colt handgun	.45	10
5	Ruger SP101 handgun	.38	9
6		.357	10
7	Rifle	.22	20
8	Rifle	.308	10
9	Remington shotgun	12ga	3
10	AR14 M4 Carbine	5.56×45mm	10
TOTAL # OF SHOTS			**102**

A total of 21 shots were fired by the .22 rifle, comprised of a set of ten (10) followed by a set of eleven (11), the latter of which was recorded with a 20-decibel (dB) amplification of the input levels. However, the amplified recordings of shot #6 were determined to be unusable, as they featured no discernible gunshot sounds.

Microphone Set-up

Twelve (12) GRAS Sound & Vibration A/S type 46DP microphone sets were utilized for the capture process. Each microphone set consisted of a type 40DP 1/8" Externally Polarized Pressure Microphone, a type 26TC ¼" preamplifier, and type 12AA and 12AG power modules providing the 200-volt polarization and 120-volt preamplifier power. The microphones provided for a ±2 dB frequency response out to 140 kHz, with a dynamic range specified between 46 dB (lower limit) and 178 dB (upper limit), resulting in an overall dynamic range of 132 dB [10].

The twelve (12) microphone sets were arranged in a semi-circular pattern along a semi-octagonal, aluminum rig having a three-meter radius. The shooting position was located at the center of the rig from an elevated position, and the microphone sets were positioned three (3) meters above the ground at 0°, 16.4°, 32.7°, 49.1°, 65.5°, 81.8°, 98.2°, 114.5°, 130.9°, 147.3°, 163.6°, and 180°, relative to the angle of fire. For purposes of this paper, these angles will be referred to as angle #1 through angle #12, respectively. Figure 4 illustrates the characteristics of the microphone rig and the relative location of the shooting position [10], while Figure 5 shows the marksman in the shooting position within the microphone rig during the capture process [11].

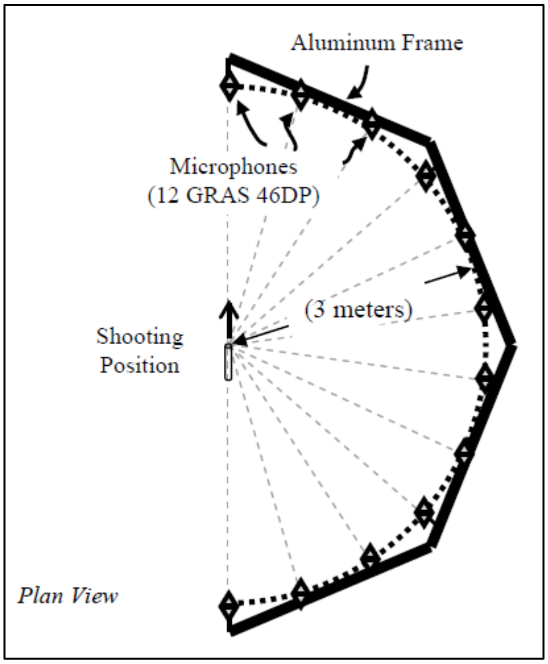

Figure 4 – Illustration of the microphone rig for the database collection process [10].

Figure 5 – Image depicting the shooter positioned in the center of the microphone rig during the database capture process [11].

Recording Characteristics

The twelve (12) microphone channels for each shot were recorded simultaneously using a National Instruments NI PXIe-1071 chassis equipped with a NI PXIe-8840 Core processor and NI PXIe-6358 data acquisition card. Each channel was recorded with 16-bit PCM encoding and with a sampling rate of 500 kHz, providing a recorded bandwidth of 250 kHz per the Nyquist sampling theorem [13]. The recorded audio for each shot was saved as a MATLAB data file (".mat"), with the twelve (12) columns in the array corresponding to the separate microphone channels from the 0° position (column 1) to the 180° position (column 12). The data values within the ".mat" files consist of the decimal equivalents of the 16-bit quantization values for each audio sample, meaning that the values range from $-(2^{15})$ or –32,768 to $(2^{15}-1)$ or 32,767.

The lengths of the recording from each angle of a shot was identical, but the lengths were not identical across all the shots. The recordings were each a multiple of one (1) second, meaning that their lengths in samples were divisible by 500,000, except for shot #8 of the SIG Sauer P239 which has a length of 2,000,001 samples (4.000002 seconds at a sampling rate of 500 kHz). The total range of lengths across the recordings was from three (3) seconds (shot #4 of the Glock 19 handgun and shots #2 and #3 of the Ruger SP101 handgun firing .38 caliber ammunition) to fifteen (15) seconds (shot #1 of the .308 caliber rifle).

METHODOLOGY

General

The overall methodology devised for this thesis can be broken down into the following phases:

1. Audio File Preparation
2. Bandwidth Reduction Through Resampling
3. Cross-Correlation Computations
4. Statistical Calculations

Audio File Preparation

Extraction of Independent Channels

The first steps for preparing the ".mat" files for use in this research were to extract each column of data (i.e., each microphone channel) as a separate vector, normalize the vector's sample values to decimal values relative to the maxima of 16-bit quantization, and then save that vector to a monaural PCM wavefile with a sampling rate of 500 kHz. With this process, a PCM wavefile was produced for each recorded angle for each shot; for the total of 102 shots, this equated to a total of 1,224 PCM wavefiles (12 angles per shot x 102 shots). Figure 6 and Figure 7 show the twelve (12) time-aligned waveform displays for shot #1 of the SIG Sauer P239 (.357) and shot #1 of the .308 caliber rifle, respectively, from 0° (top) to 180° (bottom). Note in Figure 7 that the ballistic shockwave from the supersonic bullet is seen clearly in the first three angles as the "N"-shaped signal preceding the higher-amplitude muzzle blast. As the angle between the direction of fire and the microphone increases, the time differential between the ballistic shockwave and the onset of the muzzle blast decreases.

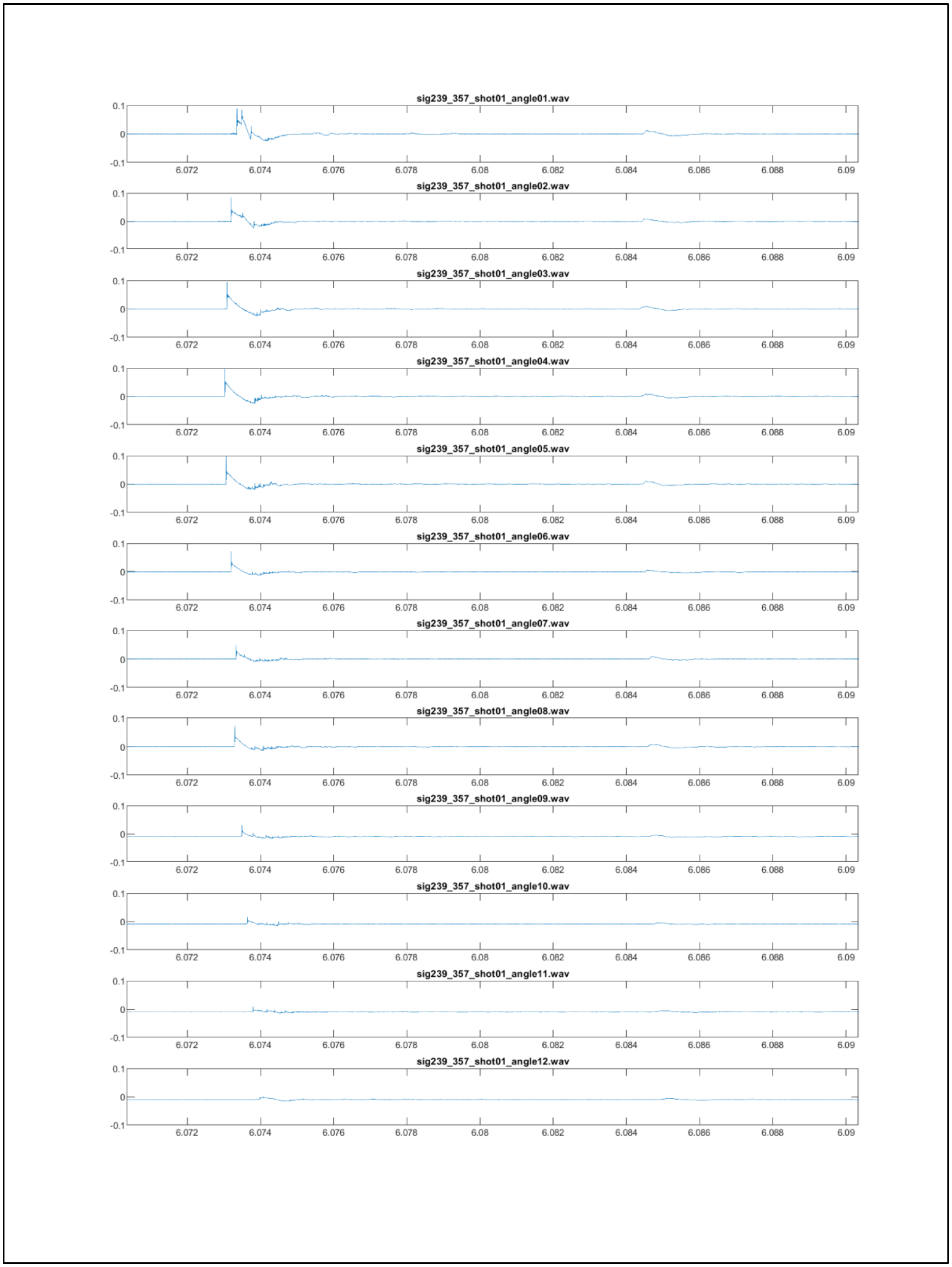

Figure 6 – Waveform displays for shot #1 of the SIG Sauer P239 (.357) from angle 1 (0°) at the top to angle 12 (180°) at the bottom. Normalized amplitude on the vertical axis versus seconds on the horizontal axis, with a total displayed length of 20 milliseconds.

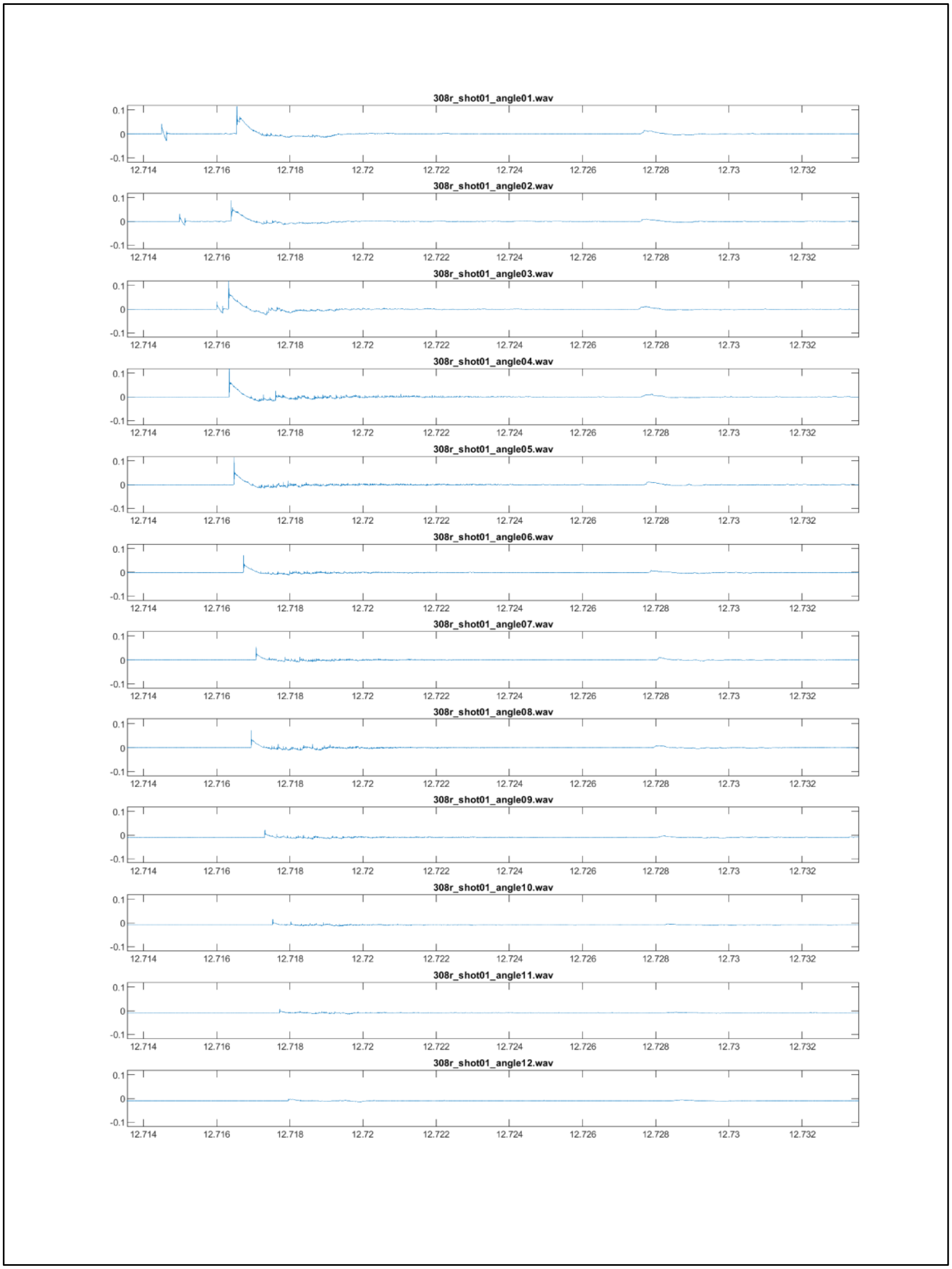

Figure 7 – Waveform displays for shot #1 of the .308 caliber rifle from angle 1 (0°) at the top to angle 12 (180°) at the bottom. Normalized amplitude on the vertical axis versus seconds on the horizontal axis, with a total displayed length of 20 milliseconds.

Direct Current Offset Removal

Direct current (DC) offset can occur in an audio recording when one (1) or more components (e.g., microphone, microphone preamplifier) induce DC voltage into the audio signal, manifesting itself as a vertical shift of the audio samples away from the x-axis [14, 15]. From review and measurement of the waveforms extracted from the source ".mat" files, it was discovered that the DC offsets of the recorded signals varied across the microphones, with the signals recorded at angles 9 through 12 exhibiting the largest offsets in the order of –300 quantization levels at 16-bit, or 0.9%. While this percentage may not be large, the cross-correlation results will be affected by the presence of the DC offset. Cross-correlation computations are immune to a scalar change of amplitude across the sample values (e.g., reducing the amplitude of an entire signal by a fixed value), but shifting the DC offset of one (1) of the signals will reduce the maximum computed cross-correlation value, especially when the overall amplitudes are lower.

To exemplify this, consider Signal X (monaural, 16-bit PCM, 8 kHz sampling rate, one-second length) which is created by frequency modulating a 60 Hz sine wave with white noise, both with peak amplitudes of –40 dB. Signal Y is created by shifting Signal X by –300 quantization levels. By definition, the autocorrelation of Signal X results in a value of +1 at lag 0 (i.e., Signal X is aligned sample-for-sample with itself when the cross-correlation computation is run). A cross-correlation computation is then run of Signals X and Y, and the result is +0.70108 at a lag of 0. The presence of DC offset reduced the maximum cross-correlation value from +1 to +0.70108. Figure 8 summarizes this example and includes graphs of the cross-correlation values versus lag values from –50 to +50.

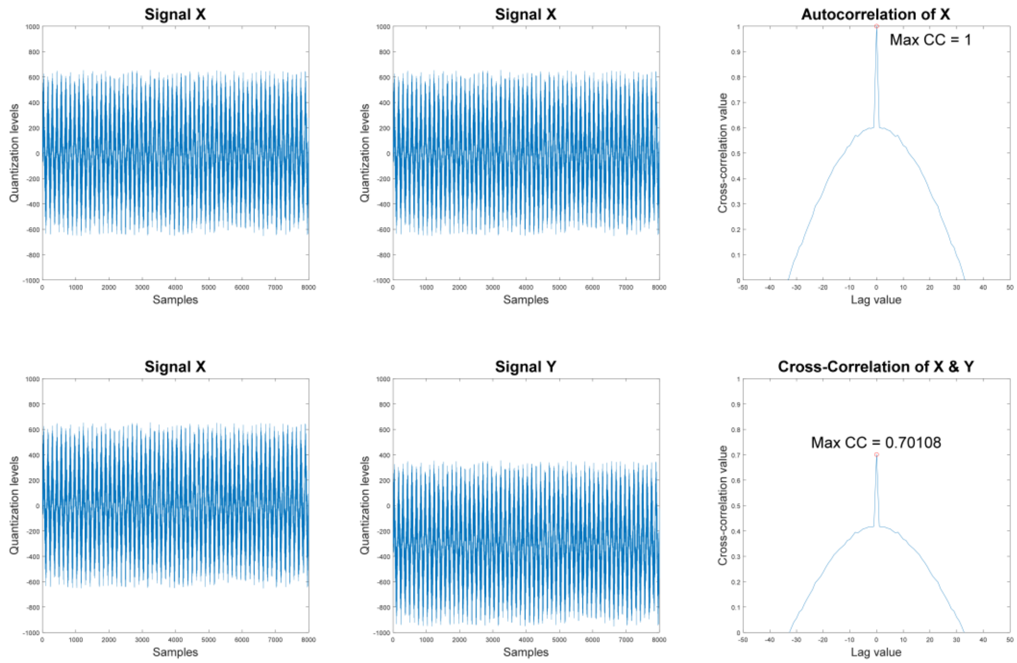

Figure 8 – Waveforms of signals X and Y, where Y is equal to X but with a –300 quantization level shift. The cross-correlation values for X/X and X/Y from lags –50 to +50 are given. The maximum cross-correlation value (at lag 0) dropped from +1 to +0.70108 with the introduction of DC offset.

Because of the negative impact that the presence of DC offset can have on the cross-correlation computations and the fact that DC offset is a channel artifact that does not convey any signal-dependent information, the wavefiles extracted from the ".mat" files were each processed to remove any DC offset present in them by performing mean subtraction and saving the results separately as new wavefiles. Mean subtraction was conducted in MATLAB R2019b using the following command, where "x" is the input signal, "x_{DC}" is the DC-corrected signal, and "n" is the total number of samples in "x":

$$x_{DC} = x - mean(x) \tag{3}$$

$$mean(x) = \frac{\sum_{i=1}^{n} x_i}{n} \tag{4}$$

Bandwidth Reduction Through Resampling

The DC offset-corrected wavefiles were downsampled from their native 500 kHz to the following sampling rates, which are all factors of 500 kHz: 250 kHz, 125 kHz, 62.5 kHz, 31.25 kHz, and 15.625 kHz. Additional downsampled wavefiles were produced at the following sampling rates, which are commonly used in professional and consumer recording systems: 192 kHz, 96 kHz, 88.2 kHz, 48 kHz, 44.1 kHz, 32 kHz, 24 kHz, 22.05 kHz, 16 kHz, 12 kHz, 11.025 kHz, and 8 kHz. In total, seventeen (17) sets of downsampled wavefiles were produced for each firearm/shot/angle recording.

The resampling processes were performed using the “resamp” function within MATLAB R2019b. The basic syntax for the “resamp” function is as follows [16]:

$$y = resamp(x, p, q[, n]) \tag{5}$$

“*y*” is the resampled output signal, “*x*” is the input signal, “*p*/*q*” is the factor by which the signal is resampled. “*n*” is an optional variable that affects the order of the antialiasing finite impulse response (FIR) lowpass filter (utilizing Kaiser windowing) employed during the resampling process, as follows [16, 17]:

$$Filter\ order = 2 \times n \times [\max(p, q)] \tag{6}$$

Generally, “*p*” is the value of the output file’s sampling rate, and “*q*” is the value of the input file’s sampling rate; however, any values which satisfy the same ratio can be used. For example, to downsample a 500 kHz signal (*x*) to a 250 kHz signal (*y*), either of the following functions could be used:

$$y = resamp(x, 250000{,}500000) \tag{7}$$

$$y = resamp(x, 1{,}2) \tag{8}$$

For the resampling processes performed in this research, the source signals were always the native 500 kHz DC-corrected wavefiles, meaning that the value of "*q*" was always 500,000. The default value of "*n*" in MATLAB R2019b is ten (10), and that value was utilized for this research [16].

Downsampling the DC-corrected, 500 kHz recordings was chosen as the process for bandwidth reduction in lieu of applying a lowpass filter. This decision was made primarily to expedite the subsequent cross-correlation computation processes. With lowpass filtering, the sampling rate of the files would remain at 500 kHz, even though the bandwidth of the recorded signal would be bandlimited; lowpass-filtered files would have required a greater number of cross-correlation computations compared to a downsampled version of the same file. As indicated above, the downsampling process inherently includes an antialiasing lowpass filter, but the resulting files do not contain the extraneous data between the cut-off frequency of the lowpass-filtered version and the original Nyquist frequency (250 kHz).

Cross-Correlation Computations

Cross-correlation computations were run of all shots within each firearm within each angle (intra-firearm, intra-angle) and for all shots across firearms within each angle (inter-firearm, intra-angle), with the process being repeated for each sampling rate from 500 kHz down to 8 kHz. For example, the three (3) recorded shots from the Remington 12-gauge shotgun were cross-correlated to each other within each angle and for each sampling rate, and then were cross-correlated with the other nine (9) firearm/caliber scenarios within each angle and for each sampling rate. No inter-angle cross-correlations were considered for this research; inter-angle comparisons have been shown to result in lower cross-correlation values and greater variance because of “[a]ngular dependence on blast size, internal ballistics, non-linear spreading, and ground reflections” [8].

For a given number of recorded shots (*n*), the formula for the number of pairs of unique intra-firearm combinations (i.e., *n* items taken two at a time with no repetitions) for each firearm (T_{intra}) is as follows [18]:

$$T_{intra} = \binom{n}{2} = \frac{n!}{2!\,(n-2)!} = \frac{n!}{2(n-2)!} \tag{9}$$

These combinations exclude the autocorrelations, which are the cross-correlations of each shot/angle recording with itself. The total number of unique, inter-firearm comparisons (T_{inter}) at each angle/sampling rate is given as the following, where 102 is the total number of shots in this study and “*n*” is the number of shots from the individual firearm (see Table 3):

$$T_{inter} = n(102 - n) \tag{10}$$

Hence, the total number of comparisons for each firearm at each angle/sampling rate ($T_{firearm\_angle}$) is the sum of T_{intra} and T_{inter}, and the total number of comparisons for each firearm across all angles ($T_{firearm\_all\_angles}$) for a given sampling rate is 12 times $T_{firearm\_angle}$. Lastly, the total number of comparisons for each firearm across all angles and across all sampling rates ($T_{firearm\_total}$) is 18 times $T_{firearm\_all\_angles}$.

Table 4 – Summary of the number of cross-correlation computations made successively for each firearm at each angle ($T_{firearm\_angle}$), across all angles ($T_{firearm\_all\_angles}$), and the total across all sampling rates ($T_{firearm\_total}$).

Firearm	**#shots (*n*)**	T_{intra}	T_{inter}	$T_{firearm\_angle}$	$T_{firearm\_all\_angles}$	$T_{firearm\_total}$
Glock 23 handgun	10	45	920	965	11,580	208,440
Glock 19 handgun	10	45	920	965	11,580	208,440
SIG Sauer P239 handgun	10	45	920	965	11,580	208,440
Colt handgun	10	45	920	965	11,580	208,440
Ruger SP101 handgun (.357)	10	45	920	965	11,580	208,440
Ruger SP101 handgun (.38)	9	36	837	873	10,476	188,568
Rifle (.22)	20	190	1,640	1,830	21,960	395,280
Rifle (.308)	10	45	920	965	11,580	208,440
Remington shotgun	3	3	297	300	3,600	64,800
AR14 M4 Carbine	10	45	920	965	11,580	208,440
TOTALS	**102**	**544**	**9,214**	**9,758**	**117,096**	**2,107,728**

The cross-correlation computations were made using the "xcorr" function within MATLAB R2019b. The basic syntax for the "xcorr" function utilized in this research was as follows [5]:

$$CC = xcorr(a, b, 'coeff') \tag{11}$$

"*a*" and "*b*" are the input wavefiles for the cross-correlation analysis, and "*CC*" is the output array containing the results of the computations. "*coeff*" refers to the method of normalization which results in the values being scaled between –1 and +1, where +1 is the autocorrelation of a signal with itself at lag 0 and –1 would be the same but with the phase of one (1) of the input signals inverted.

Normalization of the results is optional, but when a method is specified, the input signals must be of the same length. Accordingly, because the recordings in the database were not all of the same length, the maximum length of the recordings within a given set of computations was first determined, and any recordings within that set which were shorter than that maximum length were zero-padded with the appropriate number of samples. The cross-correlation computations were then carried out with pairs of files having the same length.

From the output array ("*CC*") of a given pair of wavefiles, the maximum positive cross-correlation value was identified and documented in a spreadsheet for each angle and for each sampling rate. Additionally, the corresponding lag positions for the maximum positive cross-correlation values were similarly documented in a separate set of spreadsheets by angle and sampling rate. As example sets of cross-correlation comparisons, Figure 9 displays the 500 kHz and 8 kHz intra-firearm comparisons of shot #1 with shot #2 for the 12-gauge shotgun at angle 1 (0°), aligned at the lag values which resulted in the maximum cross-correlation values and shown with a time range of twenty (20) milliseconds (i.e., 10,000 samples at 500 kHz, 160 samples at 8 kHz). Similarly, Figure 10 and Figure 11 display the same data for the shot #1/shot #3 and shot #2/shot #3 comparisons, respectively. The ground reflection in each waveform is present approximately eleven (11) milliseconds (i.e., 5,500 samples at 500 kHz, 88 samples at 8 kHz) following the onset of the respective muzzle blast.

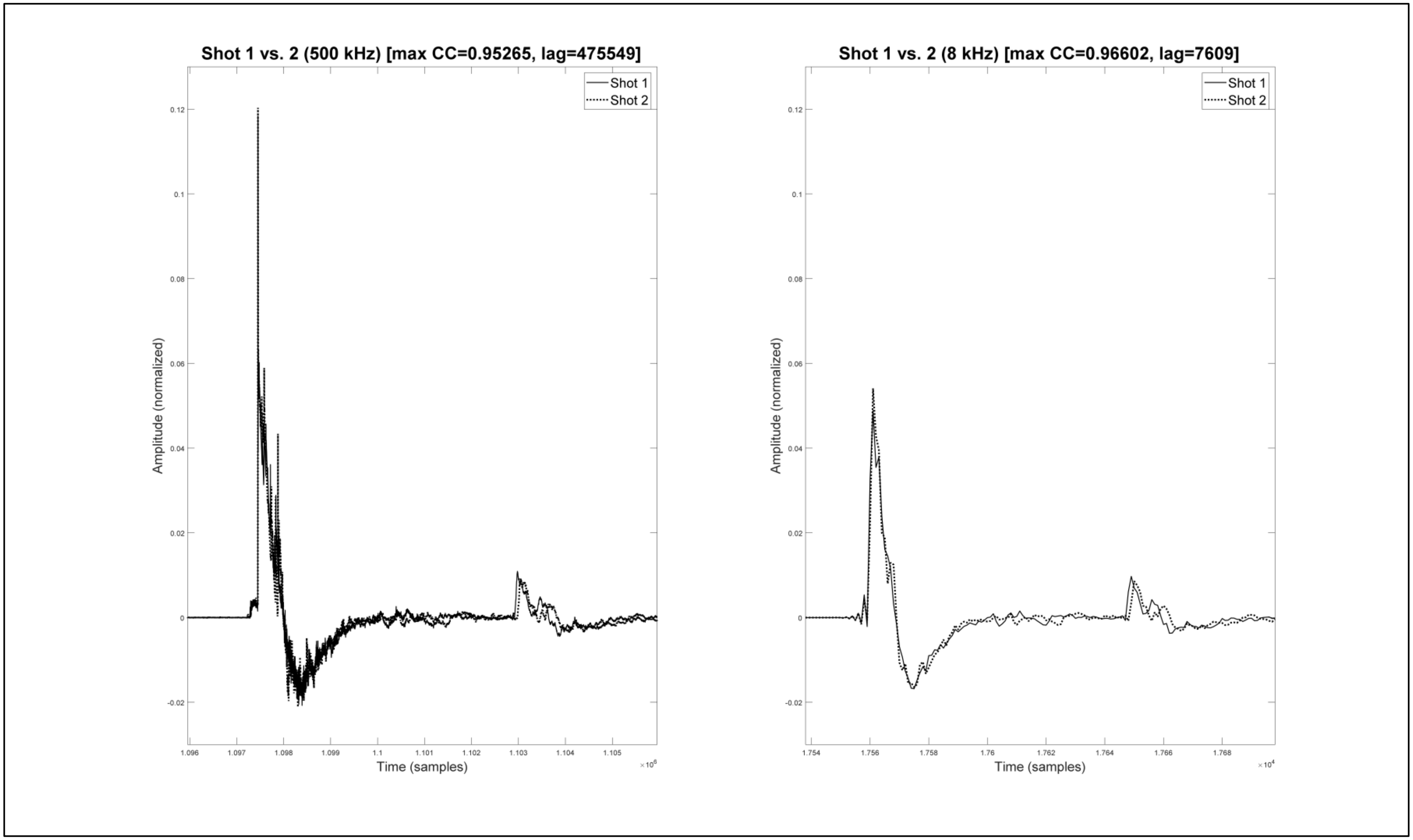

Figure 9 – The intra-firearm cross-correlation comparisons for shots #1 and #2 for angle 1 (0°) of the 12-gauge shotgun at the 500 kHz (left) and 8 kHz (right) sampling rates. Waveforms are aligned at the lag value which resulted in the maximum cross-correlation value for the respective comparison; both values are provided in the title of each plot.

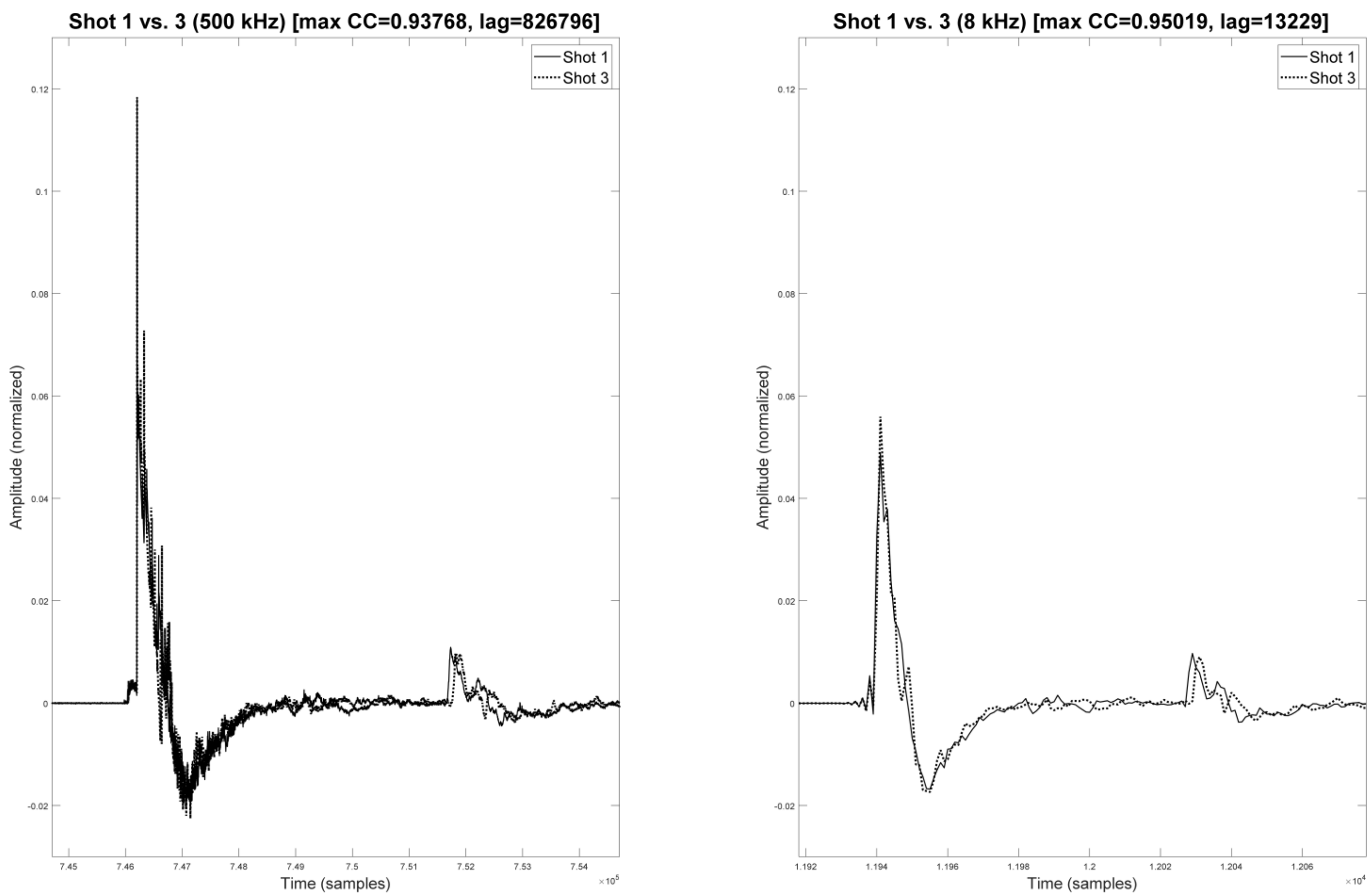

Figure 10 – The intra-firearm cross-correlation comparisons for shots #1 and #3 for angle 1 (0°) of the 12-gauge shotgun at the 500 kHz (left) and 8 kHz (right) sampling rates. Waveforms are aligned at the lag value which resulted in the maximum cross-correlation value for the respective comparison; both values are provided in the title of each plot.

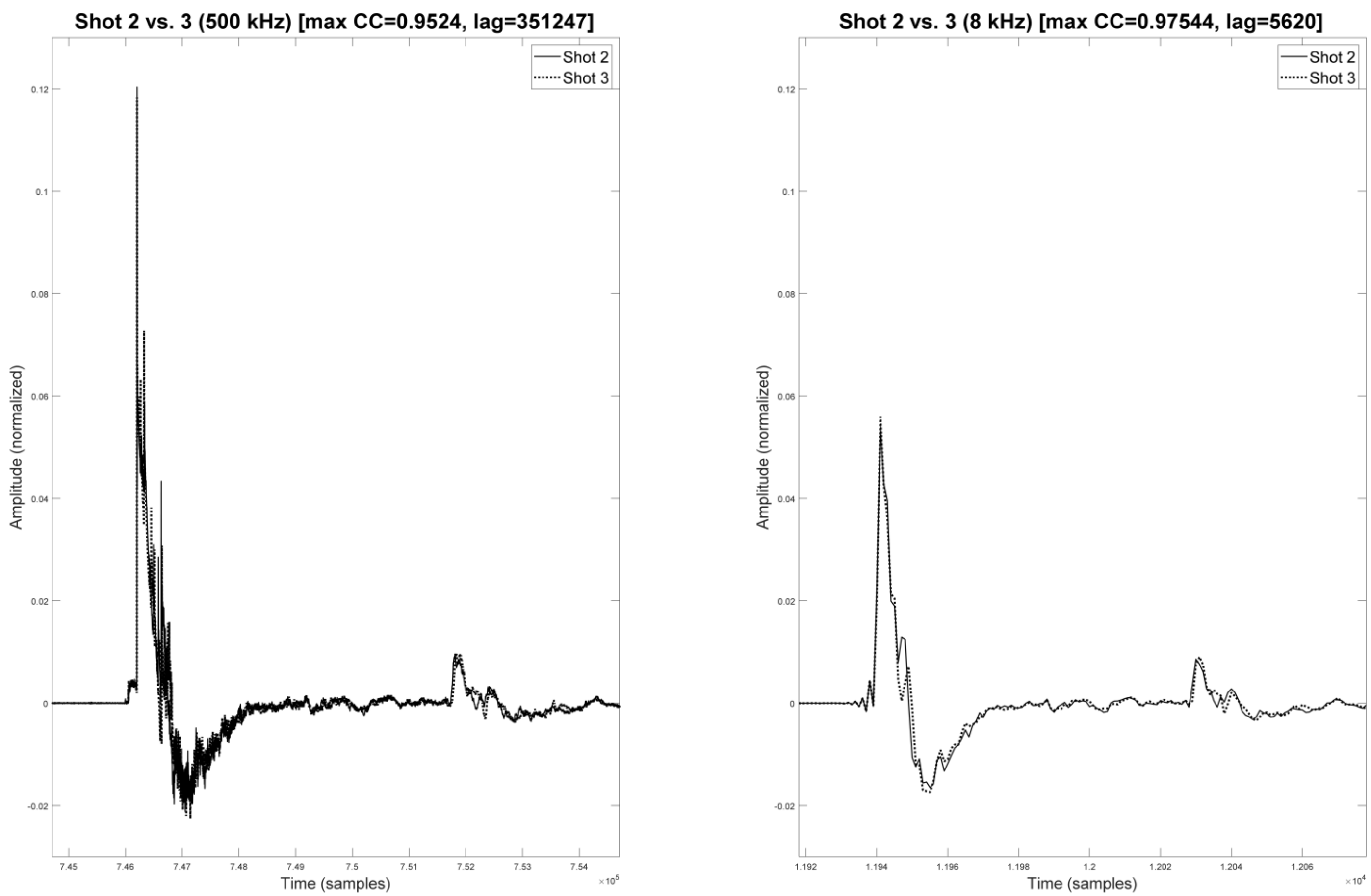

Figure 11 – The intra-firearm cross-correlation comparisons for shots #2 and #3 for angle 1 (0°) of the 12-gauge shotgun at the 500 kHz (left) and 8 kHz (right) sampling rates. Waveforms are aligned at the lag value which resulted in the maximum cross-correlation value for the respective comparison; both values are provided in the title of each plot.

Statistical Calculations

Using the maximum cross-correlation value spreadsheets, averages and standard deviation values were calculated for all intra-firearm/intra-angle comparisons and all inter-firearm/intra-angle comparisons.

For example, average and standard deviation values were calculated for the set containing all the maximum cross-correlation values for shots #1 through #3 of the Remington 12-gauge shotgun for all intra-angle comparisons (e.g., shots #1 and #2 at angle 1, shots #1 and #3 at angle 1, shots #2 and #3 at angle 1, shots #1 and #2 at angle 2, …, shots #2 and #3 at angle 12). From Table 4, there were three (3) intra-angle comparisons made for the Remington 12-gauge shotgun for each angle, or a total of 36 comparisons across the twelve (12) angles. Following that, similar average and standard deviation calculations were calculated for Remington 12-gauge shotgun shots #1 through #3 against all the intra-angle comparisons made with the other firearms. Again from Table 4, there were 297 inter-angle comparisons made for the Remington 12-gauge shotgun for each angle, or a total of 3,564 comparisons across the twelve (12) angles.

RESULTS

Table 5 and Table 6 list the computed averages and standard deviations for the maximum cross-correlation values from the intra-firearm comparisons for sampling rates 500 kHz to 44.1 kHz and 32 kHz to 8 kHz, respectively. The results are listed by firearm and for a set containing all firearms. Similarly, Table 7 and Table 8 list the same computations for the inter-firearm comparisons.

The following figures display the average maximum cross-correlation values versus sampling rate plots for the intra-firearm/intra-angle (solid blue) and inter-firearm/intra-angle (dashed orange) comparisons, as detailed below:

- Figure 12 – for all firearms
- Figure 13 – for the Remington 12-gauge shotgun
- Figure 14 – for the .22 caliber rifle
- Figure 15 – for the .308 caliber rifle
- Figure 16 – for the AR14 M4 Carbine
- Figure 17 – for the Colt handgun
- Figure 18 – for the Glock 19 handgun
- Figure 19 – for the Glock 23 handgun
- Figure 20 – for the Ruger SP101 handgun (firing .357 caliber ammunition)
- Figure 21 – for the Ruger SP101 handgun (firing .38 caliber ammunition)
- Figure 22 – for the SIG Sauer P239 handgun

Standard deviation bars are provided for each data point and are colored accordingly (blue for the intra-firearm data points and orange for the inter-firearm data points). The intra-firearm standard deviation bars are capped with an arrow, while the inter-firearm standard deviation bars are capped with a solid oval, to more easily distinguish the bars that overlap.

The percent changes for each set of sampling rates related by sequential, downward octaves (i.e., halving of the sampling rate) for all firearms are given in the following figures for both intra- and inter-firearm comparisons:

- Figure 23 – for sampling rates 500 kHz down to 15.625 kHz
- Figure 24 – for sampling rates 192 kHz down to 12 kHz
- Figure 25 – for sampling rates 88.2 kHz down to 11.025 kHz
- Figure 26 – for sampling rates 32 kHz down to 8 kHz

These percent change values were calculated per the following equation:

$$\%\ change = \frac{AvgMaxCC_{(SR/2)} - AvgMaxCC_{(SR)}}{AvgMaxCC_{(SR)}} \times 100\% \qquad (12)$$

"$AvgMaxCC_{SR}$" is the average maximum cross-correlation value at a given sampling rate ("*SR*"), and "$AvgMaxCC_{(SR/2)}$" is the average maximum cross-correlation value at half the given sampling rate (i.e., one octave down). The average maximum cross-correlation values are taken from the "All" rows of Table 5 through Table 8. For example, the percent change for the average maximum cross-correlation values from 500 kHz to 250 kHz for the intra-firearm comparisons was calculated as follows (average maximum cross-correlation values taken from Table 5):

$$\%\ change = \frac{AvgMaxCC_{(250\ kHz)} - AvgMaxCC_{(500\ kHz)}}{AvgMaxCC_{(500\ kHz)}} \times 100\% =$$

$$\frac{0.6790 - 0.5989}{0.5989} \times 100\% = 13.37\% \qquad (13)$$

Lastly, the percent changes per kHz for each successive sampling rate interval were calculated for all firearms (intra- and inter-firearm comparisons separately) as follows:

$$\frac{\%\ change}{kHz} = \frac{\left(\frac{AvgMaxCC_{(SR2)} - AvgMaxCC_{(SR1)}}{AvgMaxCC_{(SR1)}}\right)}{SR1 - SR2} \times 100\% \qquad (14)$$

"$AvgMaxCC_{SR1}$" is the starting average maximum cross-correlation value at a given sampling rate ("*SR1*", in kHz), and "$AvgMaxCC_{SR2}$" is the average maximum cross-correlation value at the ending sampling rate ("SR2", in kHz). As with equation (12) above, the average maximum cross-correlation values are taken from the "All" rows of Table 5 through Table 8. For example, the percent change per kHz for the intra-firearm, 500 kHz ("*SR1*") to 250 kHz ("*SR2*") interval comparison was derived as follows:

$$\frac{\%\ change}{kHz} = \frac{\left(\frac{AvgMaxCC_{(250\ kHz)} - AvgMaxCC_{(500\ kHz)}}{AvgMaxCC_{(500\ kHz)}}\right)}{500 - 250} \times 100\% =$$

$$\frac{\left(\frac{0.6790 - 0.5989}{0.5989}\right)}{250} \times 100\% = 0.053\,\frac{\%}{kHz} \qquad (15)$$

The percent change per kHz results are given in Figure 27 (intra-firearm comparisons) and Figure 28 (inter-firearm comparisons).

Table 5 – Average maximum cross-correlation values and their corresponding standard deviation values for the intra-firearm comparisons for sampling rates 500, 250, 192, 125, 96, 88.2, 62.5, 48 and 44.1 kHz.

INTRA-FIREARM COMPARISONS			Sampling Rate (kHz)								
Firearm	Sample size	Value	500	250	192	125	96	88.2	62.5	48	44.1
All	6,528	AVG	0.5989	0.6790	0.6963	0.7196	0.7335	0.7370	0.7490	0.7556	0.7580
		SD	0.2985	0.2372	0.2287	0.2188	0.2129	0.2114	0.2061	0.2033	0.2027
12ga shotgun	36	AVG	0.7766	0.7917	0.7967	0.8086	0.8148	0.8172	0.8215	0.8249	0.8258
		SD	0.1223	0.1121	0.1096	0.1052	0.1015	0.1013	0.0983	0.0968	0.0950
Rifle (.22)	2,280	AVG	0.2741	0.4332	0.4646	0.5014	0.5221	0.5280	0.5489	0.5613	0.5611
		SD	0.1534	0.1453	0.1525	0.1605	0.1646	0.1660	0.1715	0.1757	0.1754
Rifle (.308)	540	AVG	0.7404	0.7694	0.7769	0.7921	0.8021	0.8043	0.8120	0.8161	0.8190
		SD	0.2137	0.1839	0.1789	0.1698	0.1628	0.1614	0.1565	0.1542	0.1502
AR14 M4 Carbine	540	AVG	0.7578	0.7891	0.7979	0.8162	0.8283	0.8307	0.8393	0.8441	0.8486
		SD	0.2069	0.1738	0.1676	0.1549	0.1458	0.1438	0.1383	0.1343	0.1294
Colt	540	AVG	0.7618	0.8022	0.8129	0.8286	0.8382	0.8407	0.8472	0.8497	0.8542
		SD	0.2035	0.1714	0.1657	0.1549	0.1460	0.1446	0.1392	0.1367	0.1305
Glock 19	540	AVG	0.7291	0.7866	0.8002	0.8192	0.8312	0.8336	0.8422	0.8455	0.8504
		SD	0.2101	0.1655	0.1600	0.1481	0.1384	0.1373	0.1313	0.1298	0.1232
Glock 23	540	AVG	0.7621	0.8131	0.8251	0.8409	0.8511	0.8535	0.8597	0.8636	0.8672
		SD	0.2003	0.1596	0.1551	0.1445	0.1362	0.1350	0.1301	0.1267	0.1213
Ruger SP101 (.357)	540	AVG	0.8326	0.8541	0.8613	0.8747	0.8831	0.8856	0.8917	0.8950	0.8984
		SD	0.1320	0.1115	0.1067	0.0973	0.0912	0.0899	0.0859	0.0837	0.0794
Ruger SP101 (.38)	432	AVG	0.7611	0.8067	0.8184	0.8371	0.8490	0.8513	0.8597	0.8639	0.8680
		SD	0.1875	0.1488	0.1431	0.1324	0.1239	0.1222	0.1170	0.1142	0.1091
SIG Sauer P239	540	AVG	0.8389	0.8668	0.8740	0.8868	0.8952	0.8966	0.9021	0.9040	0.9074
		SD	0.1447	0.1172	0.1113	0.1010	0.0938	0.0924	0.0877	0.0861	0.0813

Table 6 – Average maximum cross-correlation values and their corresponding standard deviation values for the intra-firearm comparisons for sampling rates 32, 31.25, 24, 22.05, 16, 15.625, 12, 11.025, and 8 kHz.

INTRA-FIREARM COMPARISONS			Sampling Rate (kHz)								
Firearm	Sample size	Value	32	31.25	24	22.05	16	15.625	12	11.025	8
All	6,528	AVG	0.7727	0.7732	0.7775	0.7789	0.7820	0.7823	0.7835	0.7834	0.7815
		SD	0.2043	0.2039	0.2017	0.2011	0.1993	0.1992	0.1988	0.1985	0.1987
12ga shotgun	36	AVG	0.8388	0.8393	0.8422	0.8449	0.8464	0.8427	0.8454	0.8460	0.8461
		SD	0.0870	0.0873	0.0847	0.0839	0.0810	0.0833	0.0845	0.0828	0.0835
Rifle (.22)	2,280	AVG	0.5531	0.5541	0.5620	0.5645	0.5704	0.5710	0.5741	0.5737	0.5726
		SD	0.1750	0.1749	0.1773	0.1778	0.1807	0.1809	0.1850	0.1841	0.1877
Rifle (.308)	540	AVG	0.8431	0.8437	0.8466	0.8483	0.8516	0.8524	0.8545	0.8564	0.8585
		SD	0.1236	0.1235	0.1208	0.1205	0.1157	0.1163	0.1130	0.1122	0.1088
AR14 M4 Carbine	540	AVG	0.8793	0.8796	0.8836	0.8851	0.8901	0.8898	0.8952	0.8925	0.8962
		SD	0.0956	0.0949	0.0906	0.0899	0.0846	0.0849	0.0807	0.0808	0.0753
Colt	540	AVG	0.8840	0.8843	0.8860	0.8866	0.8868	0.8866	0.8875	0.8850	0.8802
		SD	0.0926	0.0924	0.0893	0.0887	0.0840	0.0832	0.0808	0.0788	0.0770
Glock 19	540	AVG	0.8855	0.8865	0.8902	0.8902	0.8922	0.8921	0.8912	0.8926	0.8900
		SD	0.0787	0.0790	0.0743	0.0749	0.0704	0.0710	0.0674	0.0672	0.0645
Glock 23	540	AVG	0.8934	0.8930	0.8939	0.8943	0.8925	0.8938	0.8924	0.8943	0.8866
		SD	0.0867	0.0864	0.0838	0.0830	0.0802	0.0807	0.0784	0.0789	0.0749
Ruger SP101 (.357)	540	AVG	0.9172	0.9175	0.9189	0.9203	0.9224	0.9221	0.9208	0.9221	0.9185
		SD	0.0595	0.0590	0.0564	0.0553	0.0528	0.0531	0.0517	0.0530	0.0537
Ruger SP101 (.38)	432	AVG	0.8981	0.8983	0.9014	0.9018	0.9047	0.9034	0.9011	0.9022	0.8999
		SD	0.0713	0.0707	0.0677	0.0672	0.0633	0.0640	0.0630	0.0627	0.0629
SIG Sauer P239	540	AVG	0.9285	0.9285	0.9303	0.9303	0.9298	0.9300	0.9287	0.9274	0.9235
		SD	0.0530	0.0526	0.0506	0.0499	0.0469	0.0469	0.0467	0.0452	0.0469

Table 7 – Average maximum cross-correlation values and their corresponding standard deviation values for the inter-firearm comparisons for sampling rates 500, 250, 192, 125, 96, 88.2, 62.5, 48 and 44.1 kHz.

INTER-FIREARM COMPARISONS			Sampling Rate (kHz)								
Firearm	**Sample size**	**Value**	**500**	**250**	**192**	**125**	**96**	**88.2**	**62.5**	**48**	**44.1**
All	110,568	AVG	0.4895	0.5395	0.5478	0.5596	0.5670	0.5690	0.5752	0.5791	0.5799
		SD	0.2815	0.2543	0.2524	0.2508	0.2498	0.2495	0.2482	0.2473	0.2478
12ga shotgun	3,654	AVG	0.4000	0.4281	0.4320	0.4378	0.4414	0.4424	0.4456	0.4473	0.4479
		SD	0.1830	0.1651	0.1634	0.1616	0.1607	0.1603	0.1593	0.1585	0.1588
Rifle (.22)	19,680	AVG	0.2013	0.2756	0.2853	0.2964	0.3035	0.3057	0.3134	0.3186	0.3164
		SD	0.0902	0.0941	0.0959	0.1017	0.1067	0.1079	0.1122	0.1155	0.1134
Rifle (.308)	11,040	AVG	0.5236	0.5619	0.5683	0.5786	0.5853	0.5870	0.5924	0.5957	0.5968
		SD	0.2629	0.2361	0.2338	0.2308	0.2288	0.2284	0.2268	0.2257	0.2255
AR14 M4 Carbine	11,040	AVG	0.5497	0.5917	0.5993	0.6118	0.6200	0.6221	0.6286	0.6325	0.6341
		SD	0.2702	0.2420	0.2394	0.2364	0.2342	0.2337	0.2318	0.2306	0.2303
Colt	11,040	AVG	0.5762	0.6240	0.6329	0.6456	0.6535	0.6555	0.6615	0.6651	0.6668
		SD	0.2748	0.2433	0.2405	0.2368	0.2341	0.2335	0.2312	0.2296	0.2295
Glock 19	11,040	AVG	0.5597	0.6153	0.6256	0.6399	0.6489	0.6512	0.6582	0.6624	0.6643
		SD	0.2664	0.2319	0.2293	0.2255	0.2228	0.2222	0.2202	0.2189	0.2186
Glock 23	11,040	AVG	0.5719	0.6252	0.6347	0.6480	0.6564	0.6585	0.6649	0.6687	0.6705
		SD	0.2674	0.2339	0.2314	0.2278	0.2253	0.2248	0.2227	0.2214	0.2210
Ruger SP101 (.357)	11,040	AVG	0.5500	0.5850	0.5915	0.6012	0.6076	0.6092	0.6142	0.6173	0.6183
		SD	0.2817	0.2588	0.2568	0.2548	0.2534	0.2530	0.2518	0.2508	0.2510
Ruger SP101 (.38)	10,044	AVG	0.5402	0.5916	0.6004	0.6131	0.6212	0.6232	0.6296	0.6336	0.6352
		SD	0.2610	0.2279	0.2252	0.2217	0.2194	0.2189	0.2171	0.2159	0.2155
SIG Sauer P239	11,040	AVG	0.5930	0.6330	0.6406	0.6519	0.6591	0.6609	0.6664	0.6696	0.6712
		SD	0.2748	0.2485	0.2462	0.2437	0.2420	0.2416	0.2400	0.2389	0.2392

Table 8 – Average maximum cross-correlation values and their corresponding standard deviation values for the inter-firearm comparisons for sampling rates 32, 31.25, 24, 22.05, 16, 15.625, 12, 11.025, and 8 kHz.

INTER-FIREARM COMPARISONS			Sampling Rate (kHz)								
Firearm	**Sample size**	**Value**	**32**	**31.25**	**24**	**22.05**	**16**	**15.625**	**12**	**11.025**	**8**
All	110,568	AVG	0.5891	0.5894	0.5925	0.5934	0.5966	0.5968	0.5992	0.5998	0.6020
		SD	0.2514	0.2513	0.2503	0.2500	0.2490	0.2490	0.2486	0.2487	0.2478
12ga shotgun	3,654	AVG	0.4531	0.4535	0.4546	0.4551	0.4560	0.4562	0.4569	0.4566	0.4572
		SD	0.1610	0.1609	0.1602	0.1599	0.1593	0.1591	0.1585	0.1583	0.1581
Rifle (.22)	19,680	AVG	0.3069	0.3074	0.3118	0.3130	0.3174	0.3175	0.3206	0.3209	0.3239
		SD	0.1054	0.1057	0.1082	0.1090	0.1127	0.1128	0.1168	0.1177	0.1211
Rifle (.308)	11,040	AVG	0.6069	0.6072	0.6097	0.6105	0.6132	0.6133	0.6155	0.6159	0.6174
		SD	0.2235	0.2234	0.2222	0.2218	0.2205	0.2203	0.2197	0.2195	0.2178
AR14 M4 Carbine	11,040	AVG	0.6475	0.6478	0.6511	0.6522	0.6557	0.6559	0.6589	0.6596	0.6632
		SD	0.2294	0.2293	0.2280	0.2276	0.2262	0.2262	0.2254	0.2255	0.2244
Colt	11,040	AVG	0.6818	0.6821	0.6847	0.6856	0.6878	0.6880	0.6899	0.6904	0.6917
		SD	0.2289	0.2288	0.2270	0.2266	0.2245	0.2244	0.2228	0.2226	0.2203
Glock 19	11,040	AVG	0.6814	0.6817	0.6853	0.6864	0.6901	0.6902	0.6932	0.6937	0.6963
		SD	0.2169	0.2168	0.2156	0.2152	0.2136	0.2135	0.2124	0.2125	0.2105
Glock 23	11,040	AVG	0.6859	0.6862	0.6888	0.6894	0.6918	0.6917	0.6935	0.6944	0.6954
		SD	0.2194	0.2192	0.2179	0.2173	0.2159	0.2157	0.2150	0.2149	0.2132
Ruger SP101 (.357)	11,040	AVG	0.6284	0.6286	0.6312	0.6320	0.6347	0.6350	0.6374	0.6378	0.6407
		SD	0.2512	0.2511	0.2501	0.2497	0.2485	0.2483	0.2476	0.2473	0.2464
Ruger SP101 (.38)	10,044	AVG	0.6486	0.6489	0.6522	0.6533	0.6574	0.6578	0.6612	0.6624	0.6654
		SD	0.2136	0.2136	0.2123	0.2121	0.2112	0.2112	0.2112	0.2113	0.2100
SIG Sauer P239	11,040	AVG	0.6849	0.6851	0.6878	0.6885	0.6909	0.6913	0.6931	0.6935	0.6948
		SD	0.2405	0.2402	0.2390	0.2387	0.2372	0.2373	0.2365	0.2366	0.2360

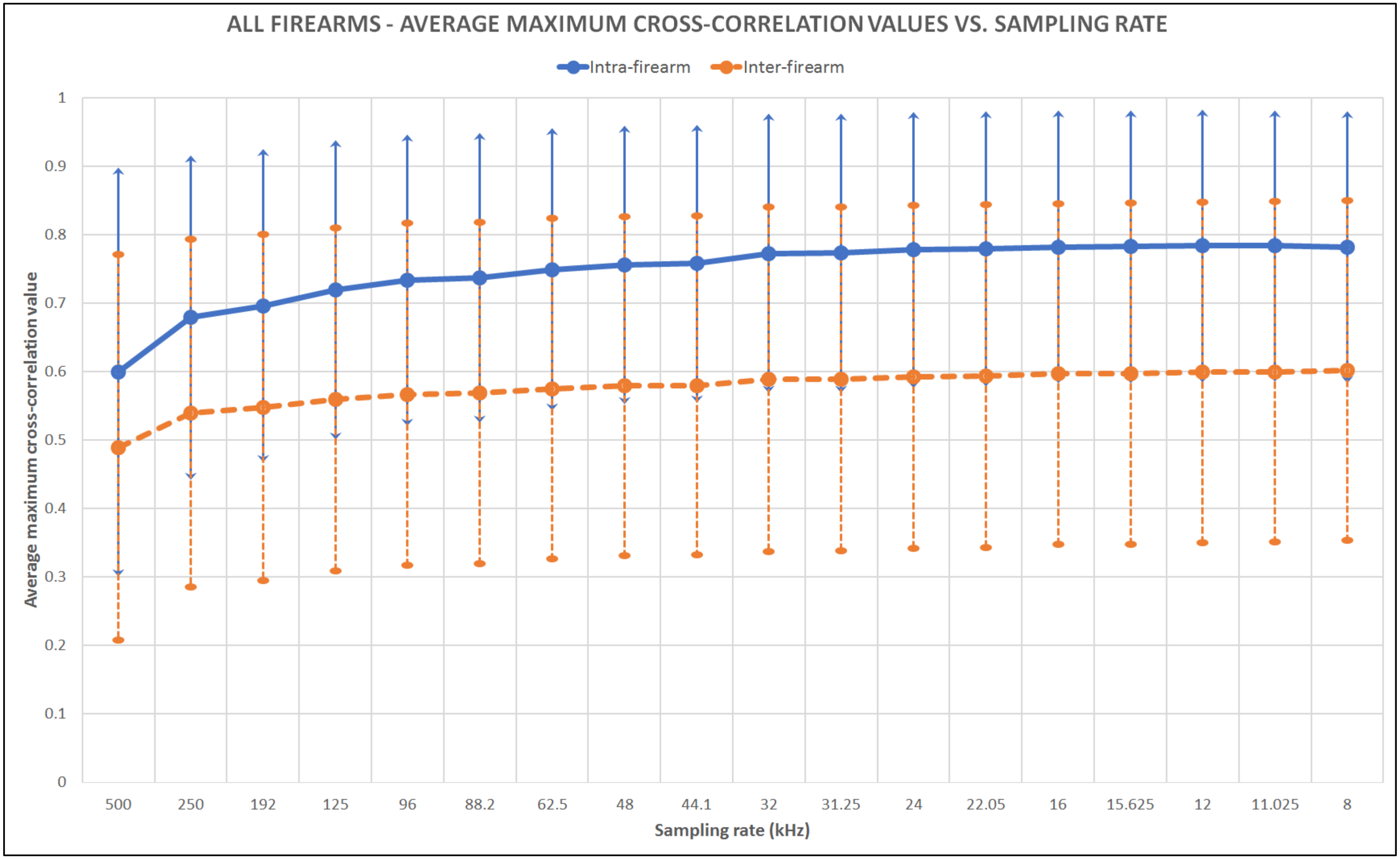

Figure 12 – Average maximum cross-correlation results vs. sampling rate for all firearms. Solid blue plot is the intra-firearm computations, and dashed orange plot is the inter-firearm computations. Standard deviation bars shown for each plot.

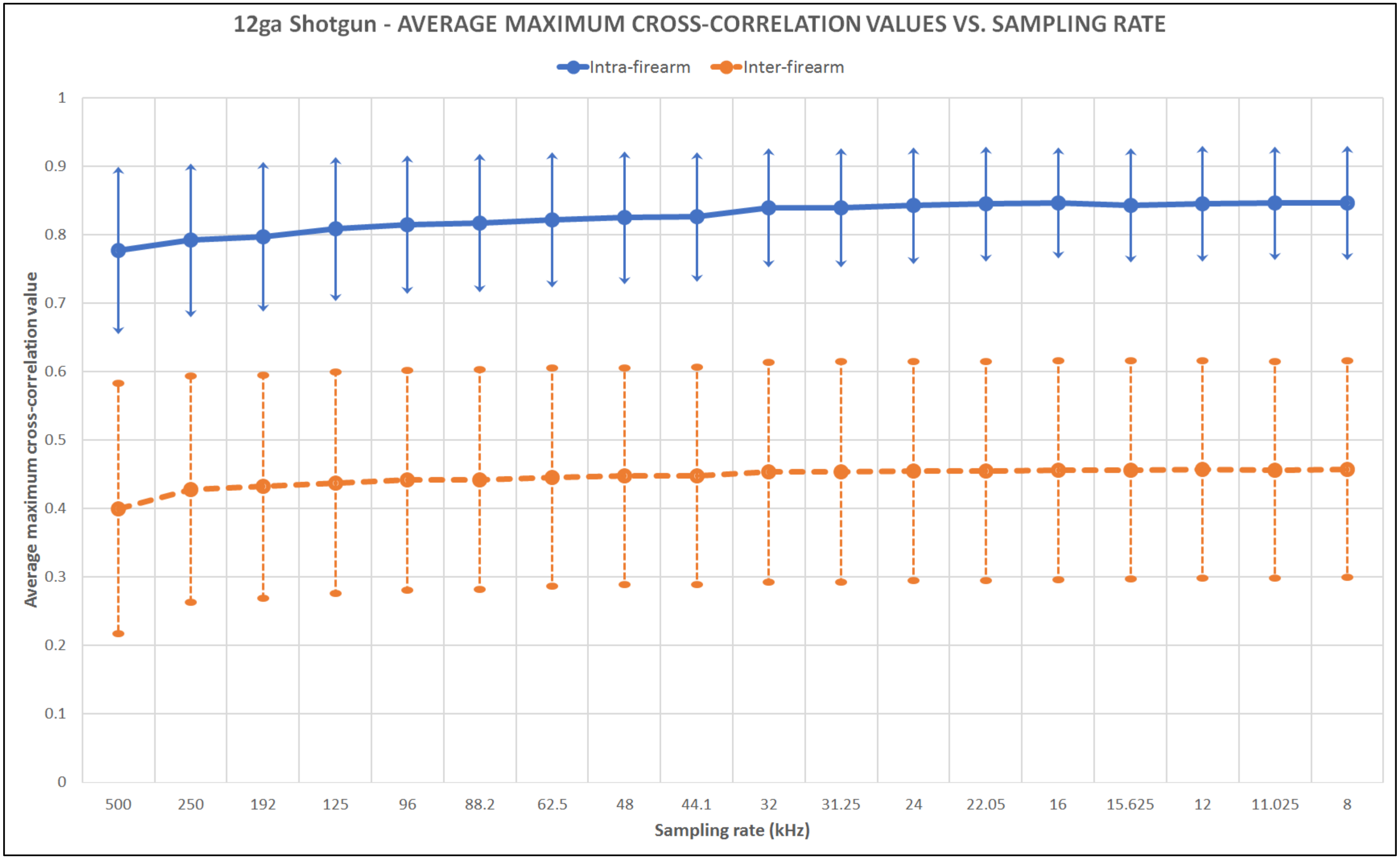

Figure 13 – Average maximum cross-correlation results vs. sampling rate for the 12-gauge shotgun. Solid blue plot is the intra-firearm computations, and dashed orange plot is the inter-firearm computations. Standard deviation bars shown for each plot.

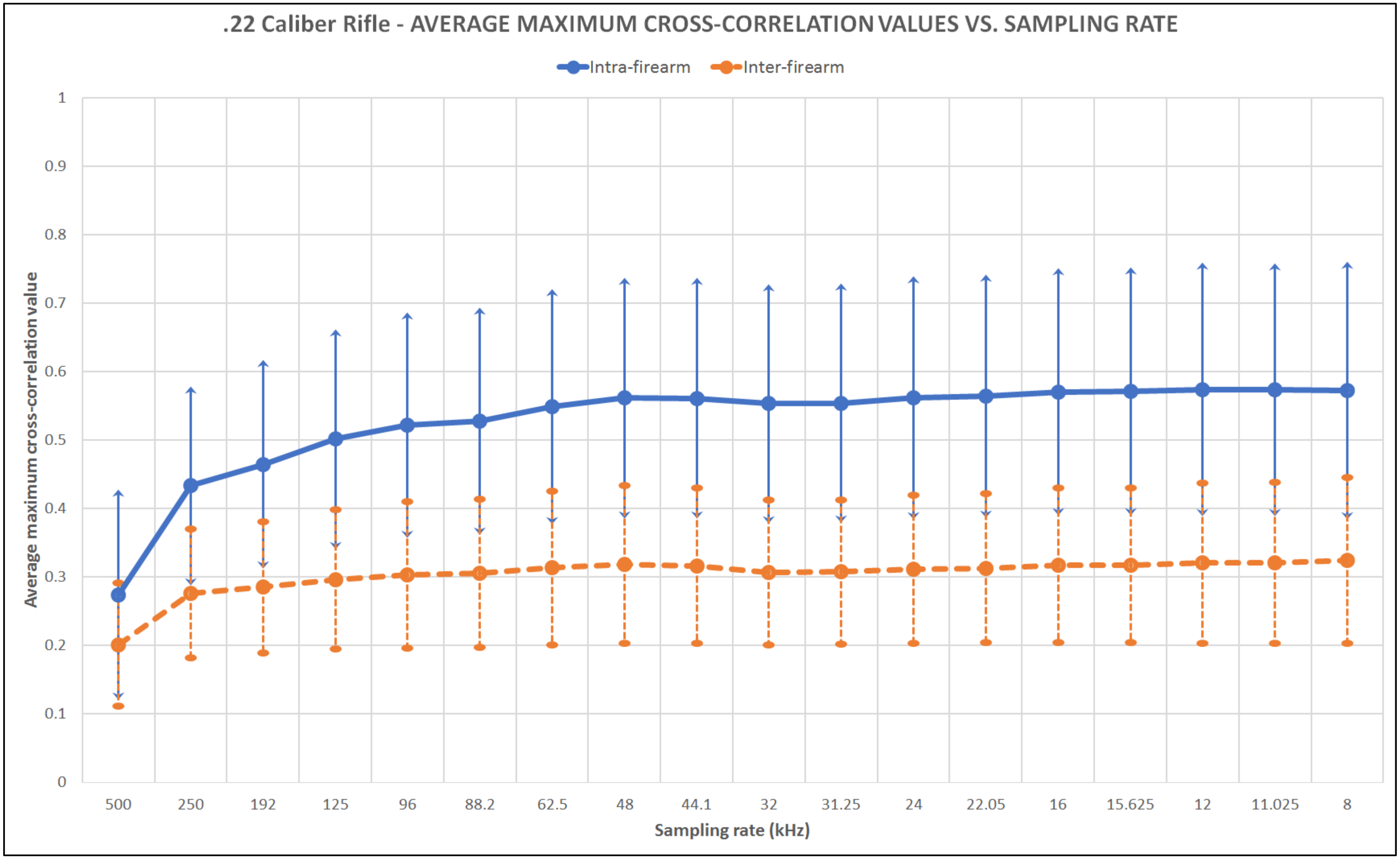

Figure 14 – Average maximum cross-correlation results vs. sampling rate for the .22 caliber rifle. Solid blue plot is the intra-firearm computations, and dashed orange plot is the inter-firearm computations. Standard deviation bars shown for each plot.

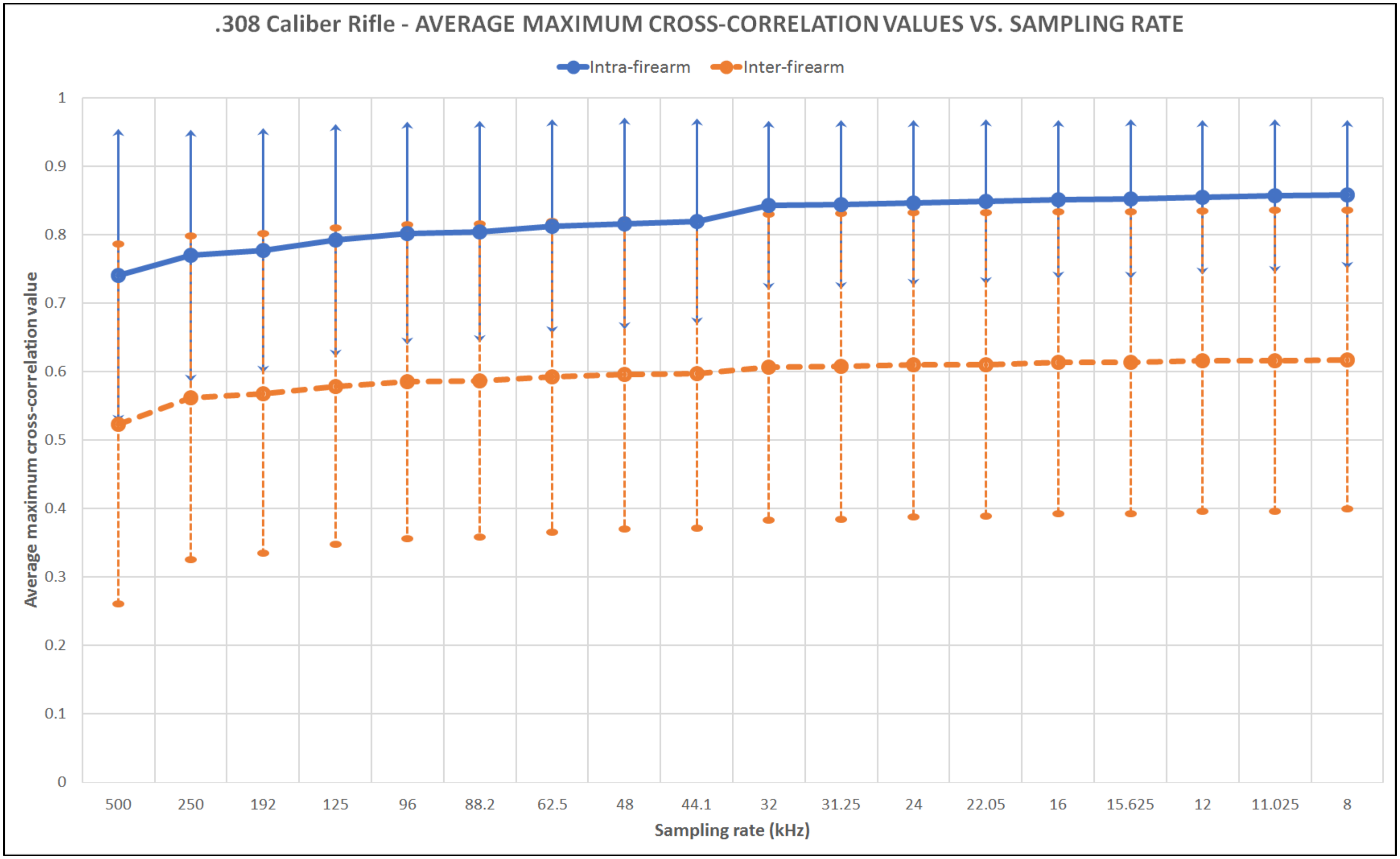

Figure 15 – Average maximum cross-correlation results vs. sampling rate for the .308 caliber rifle. Solid blue plot is the intra-firearm computations, and dashed orange plot is the inter-firearm computations. Standard deviation bars shown for each plot.

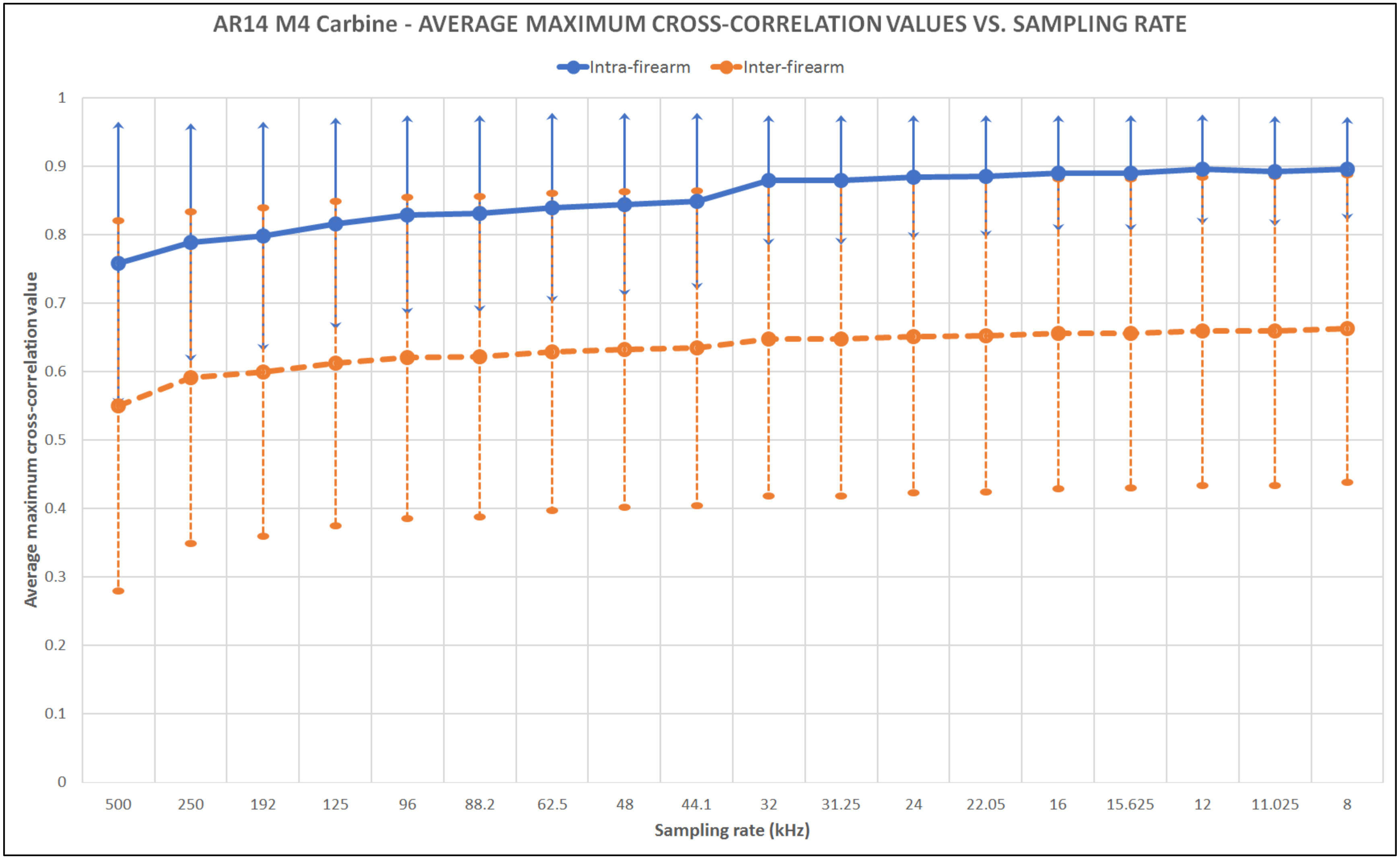

Figure 16 – Average maximum cross-correlation results vs. sampling rate for the AR14 M4 Carbine. Solid blue plot is the intra-firearm computations, and dashed orange plot is the inter-firearm computations. Standard deviation bars shown for each plot.

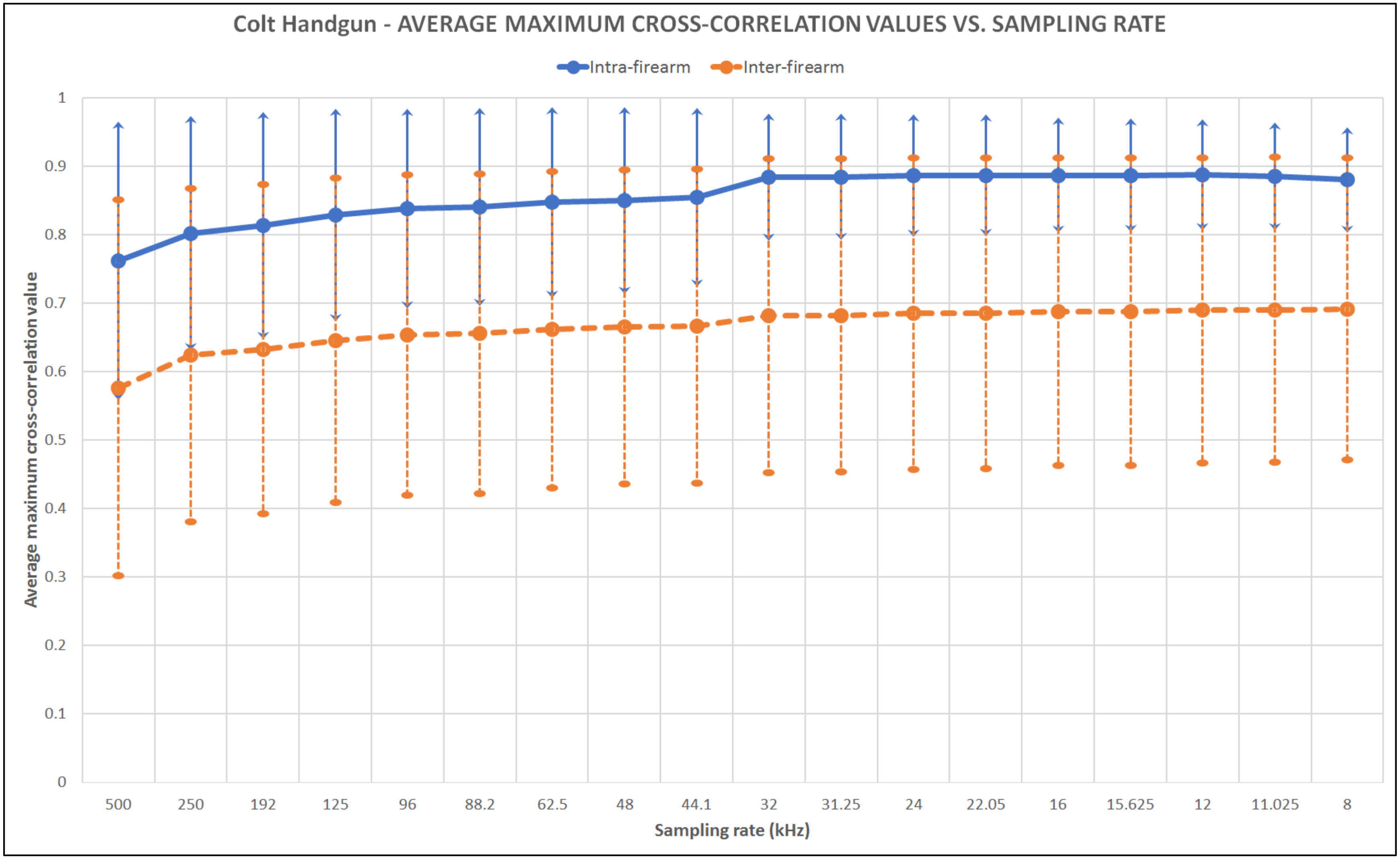

Figure 17 – Average maximum cross-correlation results vs. sampling rate for the Colt handgun. Solid blue plot is the intra-firearm computations, and dashed orange plot is the inter-firearm computations. Standard deviation bars shown for each plot.

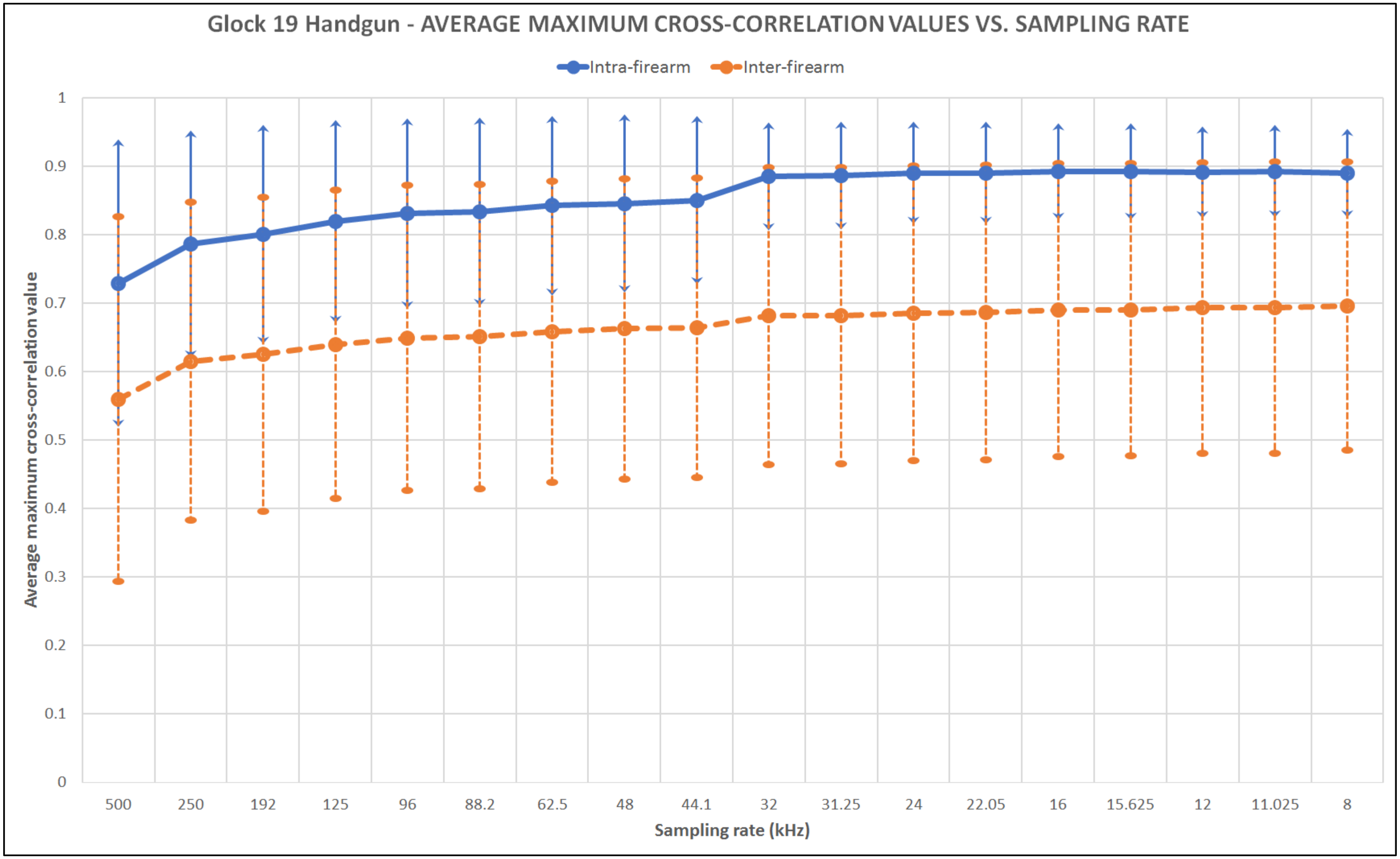

Figure 18 – Average maximum cross-correlation results vs. sampling rate for the Glock 19 handgun. Solid blue plot is the intra-firearm computations, and dashed orange plot is the inter-firearm computations. Standard deviation bars shown for each plot.

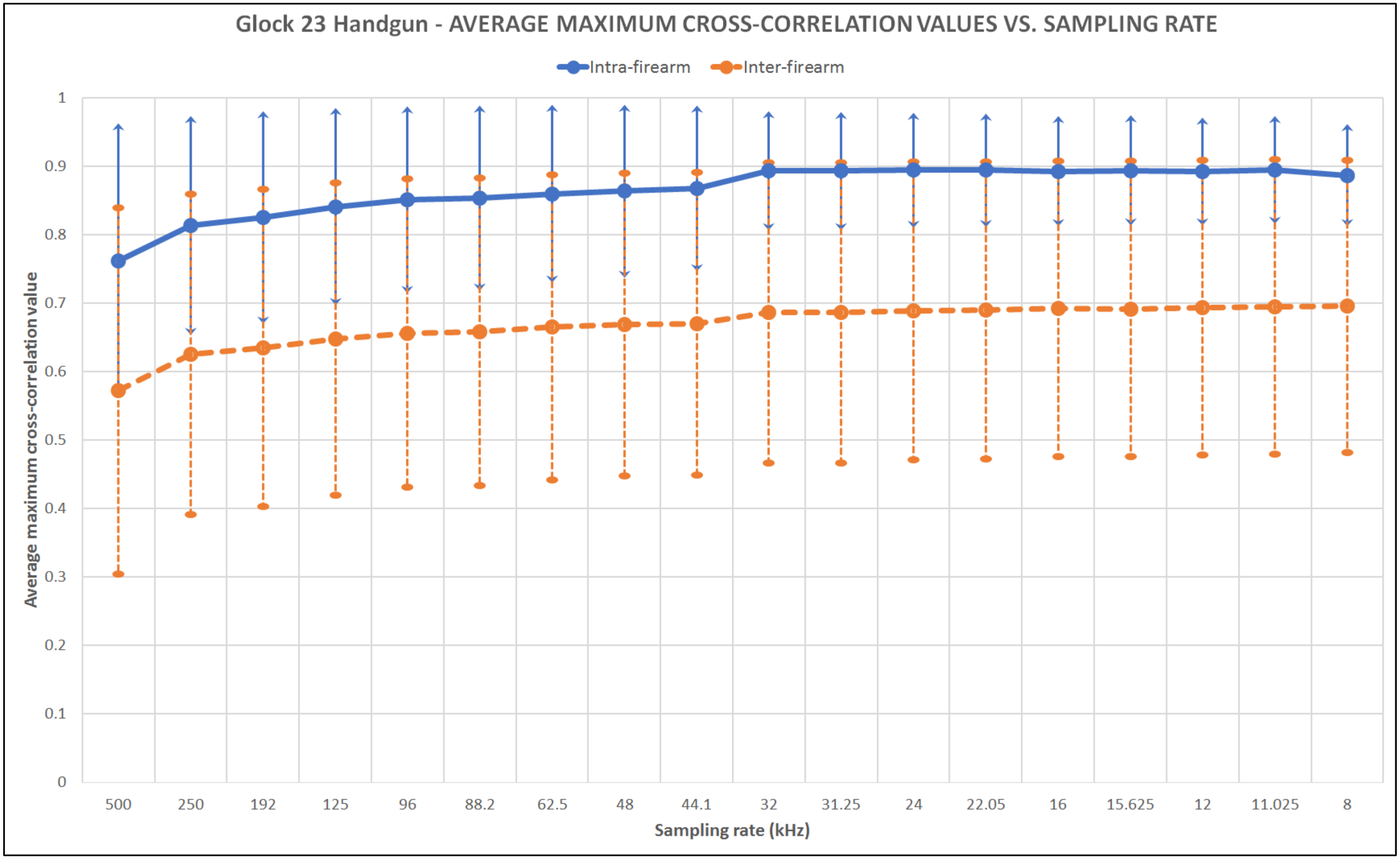

Figure 19 – Average maximum cross-correlation results vs. sampling rate for the Glock 23 handgun. Solid blue plot is the intra-firearm computations, and dashed orange plot is the inter-firearm computations. Standard deviation bars shown for each plot.

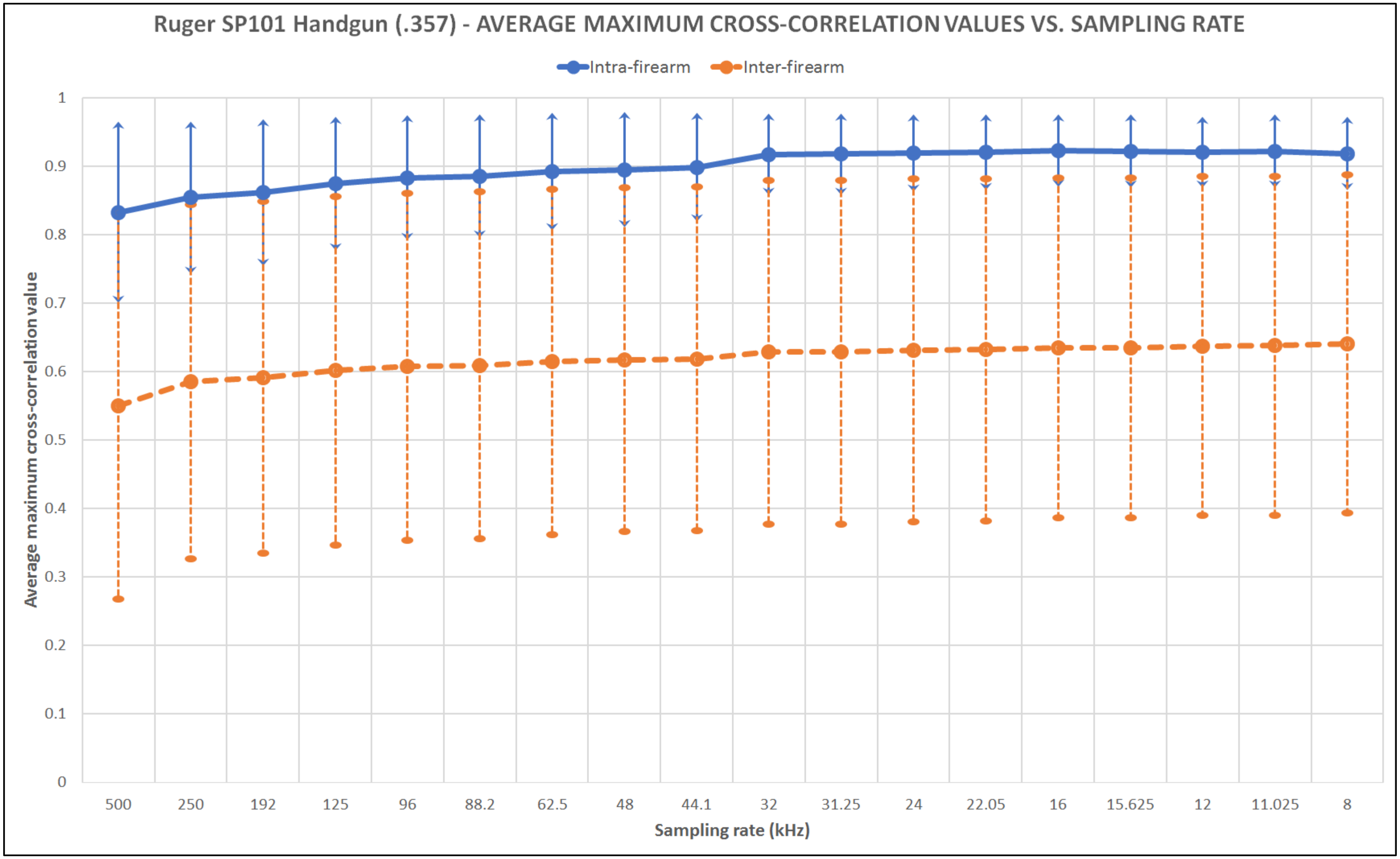

Figure 20 – Average maximum cross-correlation results vs. sampling rate for the Ruger SP101 handgun (.357). Solid blue plot is the intra-firearm computations, and dashed orange plot is the inter-firearm computations. Standard deviation bars shown for each plot.

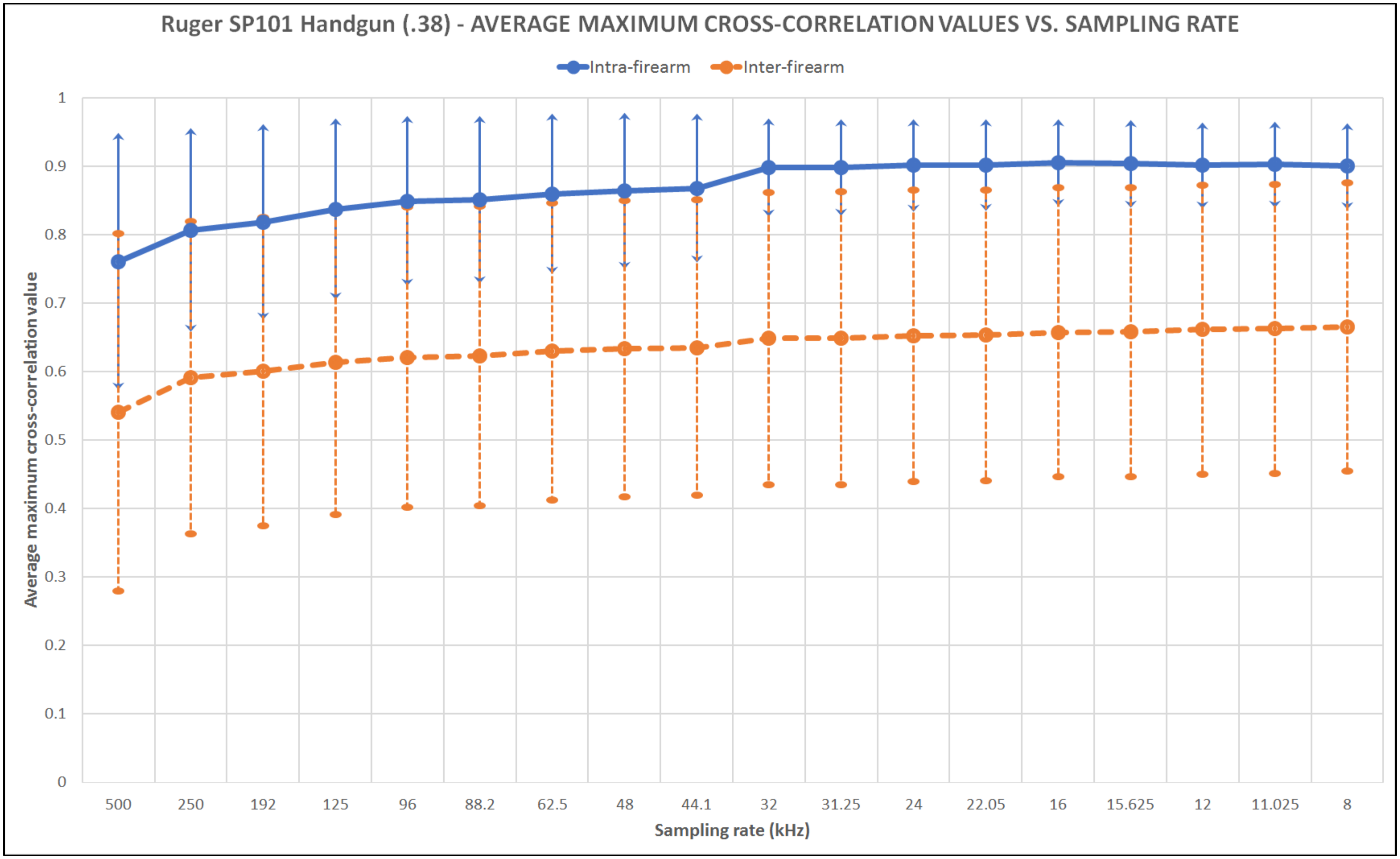

Figure 21 – Average maximum cross-correlation results vs. sampling rate for the Ruger SP101 handgun (.38). Solid blue plot is the intra-firearm computations, and dashed orange plot is the inter-firearm computations. Standard deviation bars shown for each plot.

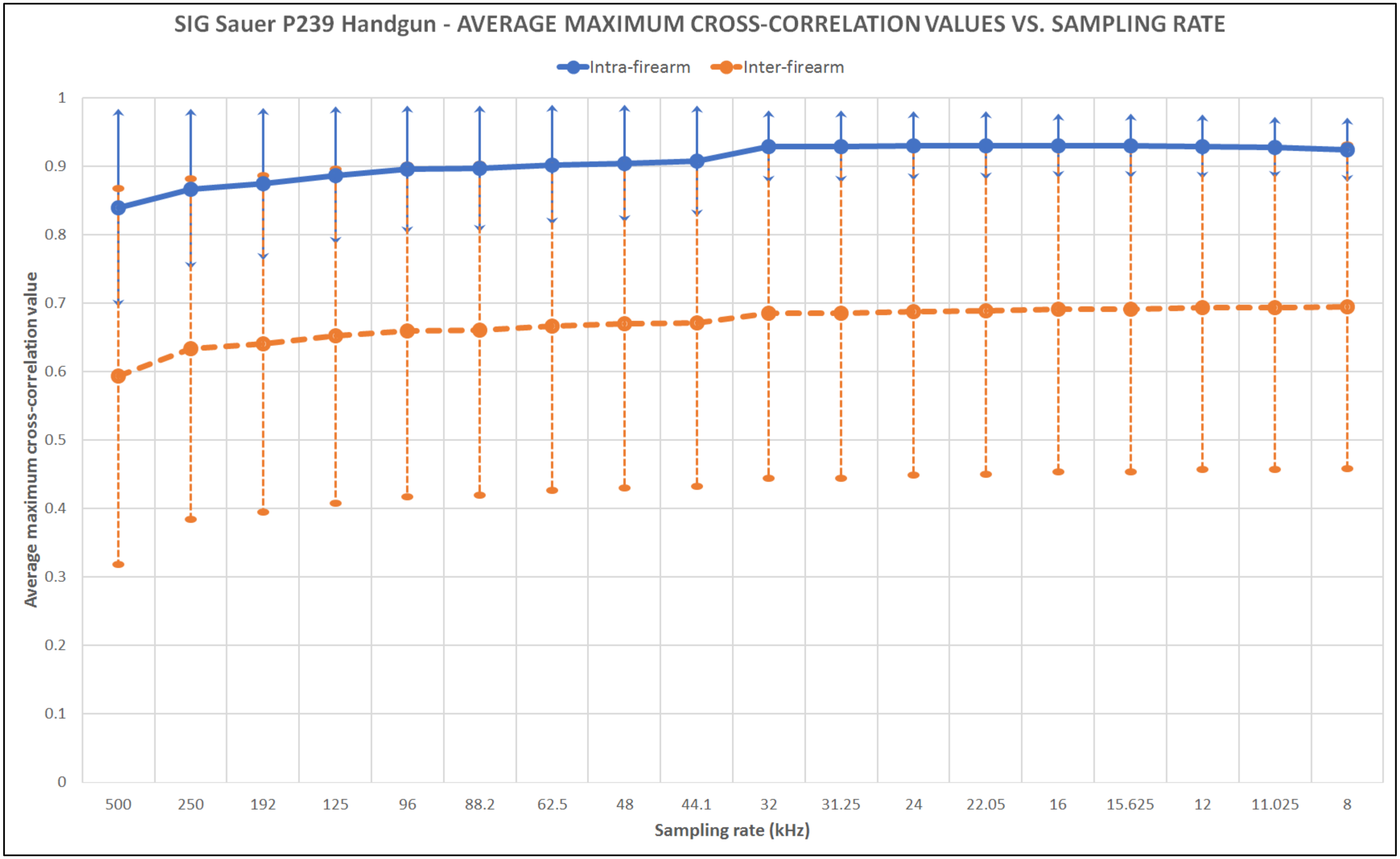

Figure 22 – Average maximum cross-correlation results vs. sampling rate for the SIG Sauer P239 handgun. Solid blue plot is the intra-firearm computations, and dashed orange plot is the inter-firearm computations. Standard deviation bars shown for each plot.

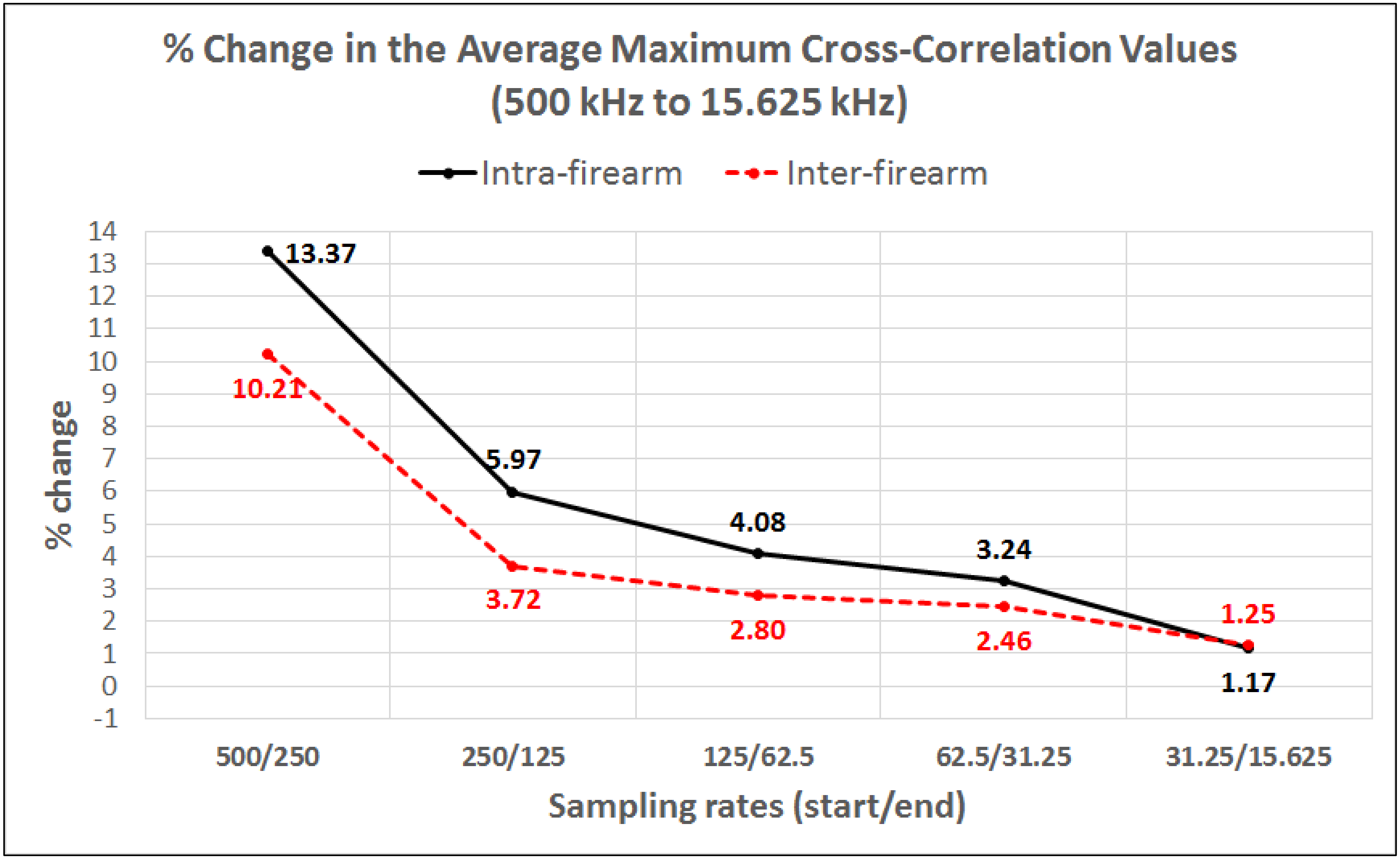

Figure 23 – Percent changes in the average maximum cross-correlation values for sampling rates 500 kHz down to 15.625 kHz in downward octave steps. Solid black plot represents the intra-firearm values, and dashed red plot represents the inter-firearm values.

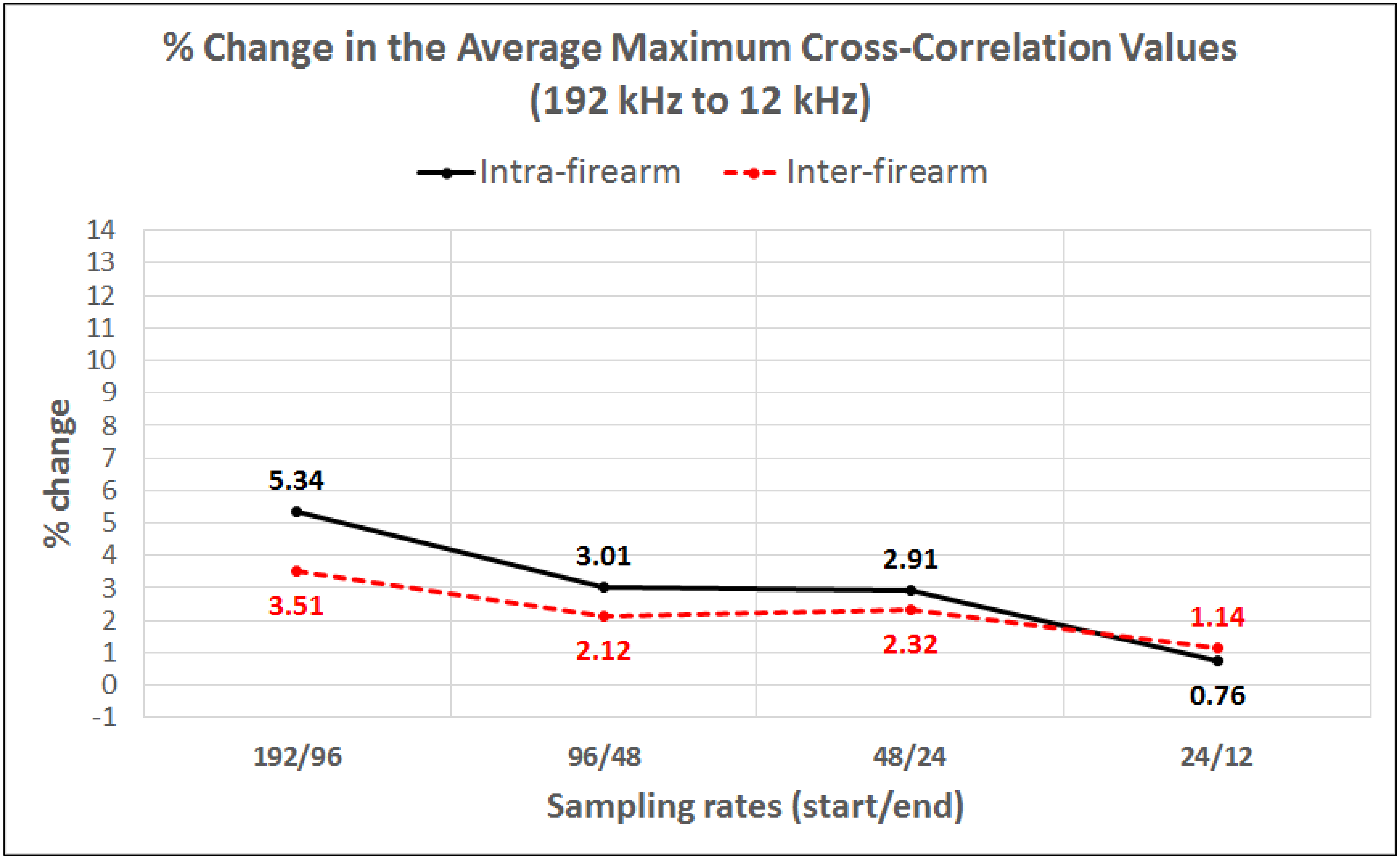

Figure 24 – Percent changes in the average maximum cross-correlation values for sampling rates 192 kHz down to 12 kHz in downward octave steps. Solid black plot represents the intra-firearm values, and dashed red plot represents the inter-firearm values.

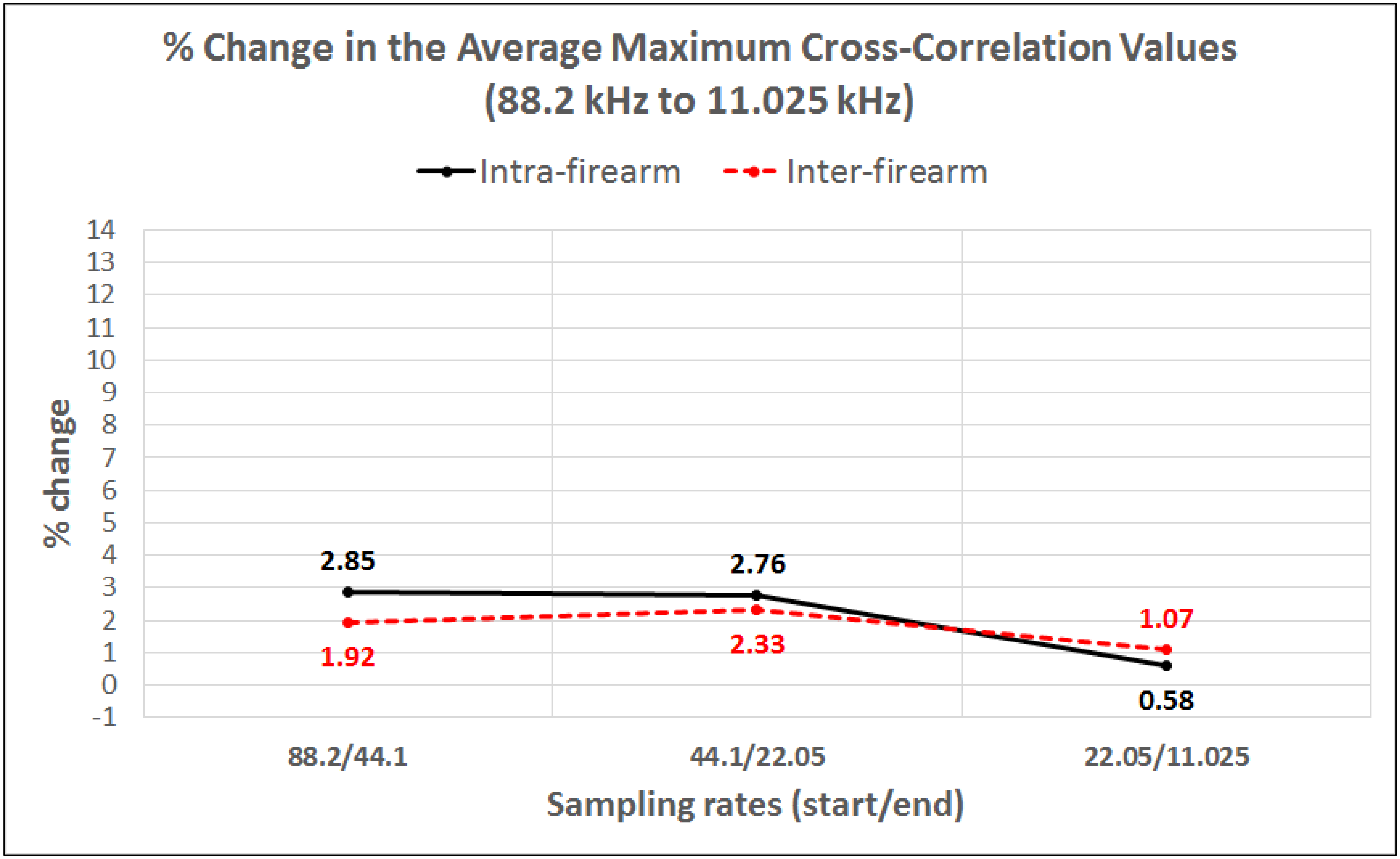

Figure 25 – Percent changes in the average maximum cross-correlation values for sampling rates 88.2 kHz down to 11.025 kHz in downward octave steps. Solid black plot represents the intra-firearm values, and dashed red plot represents the inter-firearm values.

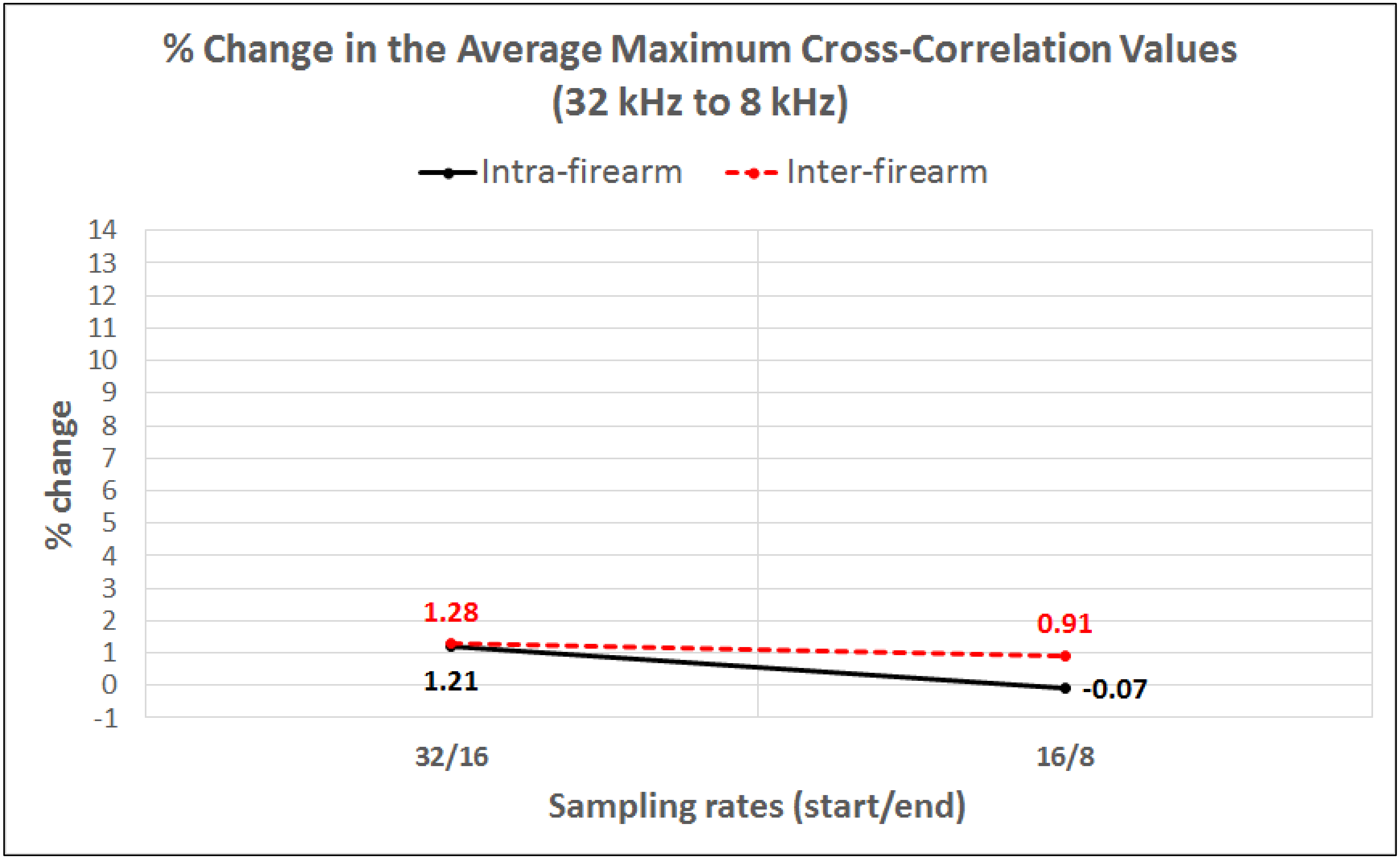

Figure 26 – Percent changes in the average maximum cross-correlation values for sampling rates 32 kHz down to 8 kHz in downward octave steps. Solid black plot represents the intra-firearm values, and dashed red plot represents the inter-firearm values.

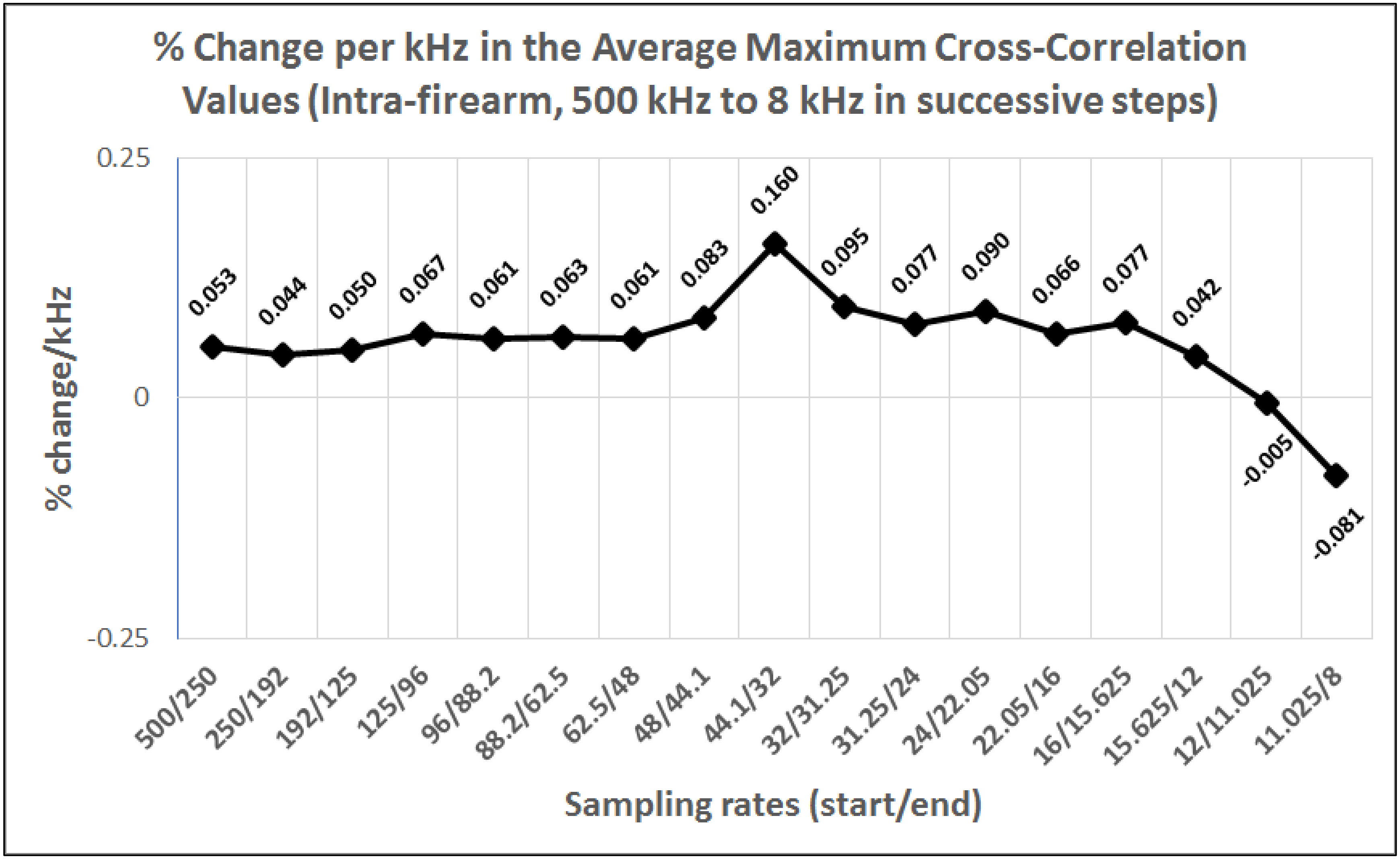

Figure 27 – Percent changes per kHz in the average maximum cross-correlation values for the intra-firearm comparisons in successive sampling rate steps.

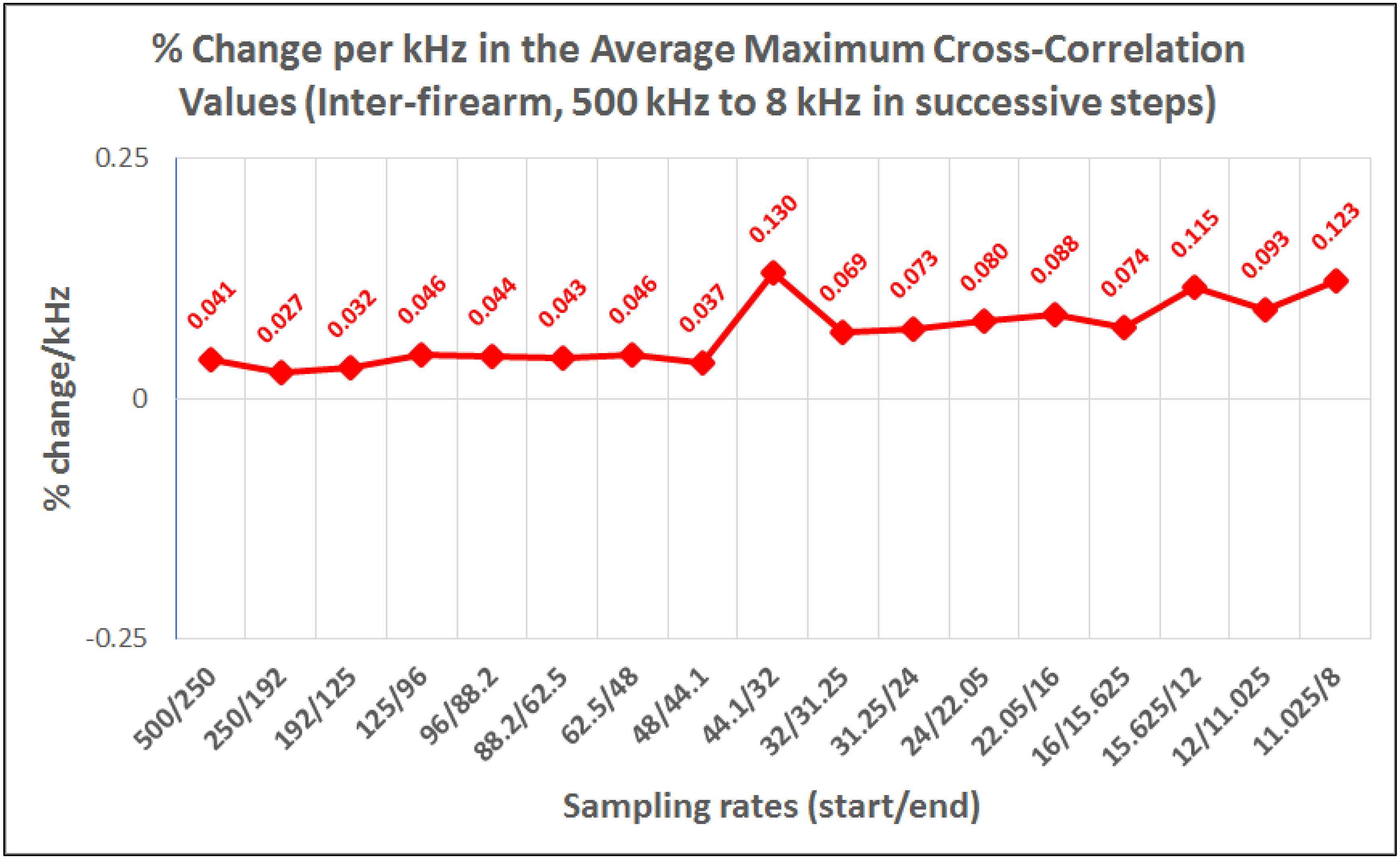

Figure 28 – Percent changes per kHz in the average maximum cross-correlation values for the inter-firearm comparisons in successive sampling rate steps.

CONCLUSIONS

The results of the research conducted for this thesis support the hypotheses that as the bandwidth of an audio recording is decreased, the corresponding maximum cross-correlation values will increase for both intra- and inter-firearm comparisons.

Except for the transition from 16 kHz to 8 kHz for the intra-firearm condition, all the percent changes in the average maximum cross-correlation computations for the octave-interval results were positive (see Figure 23, Figure 24, Figure 25, and Figure 26). The greatest percent change was observed in the 500 kHz to 250 kHz transition for both intra- and inter-firearm comparisons. The percent changes generally decreased as the sampling rates decreased; however, there were two (2) instances in the inter-firearm percent changes where successive values slightly increased (from 2.12% to 2.32% for the transition between 96 kHz/48 kHz and 48 kHz/24 kHz, and from 1.92% to 2.33% for the transition between 88.2 kHz/44.1 kHz and 44.1 kHz/22.05 kHz).

The results of the successive sampling rate percent changes per kHz revealed positive results for all the intra- and inter-firearm comparison intervals, except for the last two (2) transitions of the intra-firearm results (–0.005%/kHz for the 12 kHz/11.025 kHz transition and –0.081%/kHz for the 11.025 kHz to 8 kHz transition). Both the intra- and inter-firearm results exhibit a noticeable peak at the 44.1 kHz to 32 kHz transition, the reason for which is not readily apparent.

As indicated above in the “Research Focus section”, the primary reason for the increases in the maximum cross-correlation values is likely the systematic removal of the high-frequency variations in the recorded gunshots as the sampling rate (and therefore, bandwidth) is reduced.

The cumulative effect of the differences in these high-frequency variations results in minor but quantified differences in the corresponding cross-correlation values.

For the individual firearm computations, the only firearm which exhibited a clear separation between the intra- and inter-firearm plots of the average maximum cross-correlation values (i.e., no overlap of their standard deviation ranges) was the Remington 12-gauge shotgun (see Figure 13). The intra- and inter-firearm plots for all other individual firearms and for the set of all firearms overlap within one (1) standard deviation. The mechanisms by which the shotgun discharges and the differences in its ammunition type, relative to the handguns and rifles, likely led to its shots being more distinctive among the set of tested firearms.

It was noted that the intra-firearm results for the .22 caliber rifle never exceeded 0.6 (not including the standard deviation range), which was relatively poor compared to the other firearms which always exceeded 0.7. Similarly, the inter-firearm results for the .22 caliber rifle were lower overall than the other firearms' results, with the maximum being 0.3239 at 8 kHz; whereas the other firearms ranged from 0.4572 (Remington 12-gauge shotgun) to 0.6963 (Glock 19) for the inter-firearm results at 8 kHz. These results may have resulted from the inclusion of the initial set of ten (10) shots from the .22 caliber rifle, which exhibited poorer signal-to-noise than the subsequent set of eleven (11) shots with the 20-dB amplification.

The standard deviation ranges for the intra-firearm computations for all firearms generally decreased as the sampling rate decreased, with the .22 caliber rifle and Remington 12-gauge shotgun exhibiting the lowest rates of change. For the inter-firearm computations, the differences in the standard deviation ranges also decreased but were not as significant as the intra-firearm results, which may be due to the inclusion of different firearm classes (e.g., handguns, rifles, shotgun) in the test set.

The hypothesis regarding the decreases in bandwidth compromising the ability to statistically distinguish between recorded gunshot sounds from different firearms is not supported by the data in this research. As observed in Figure 12 through Figure 22, the overlaps in the intra- and inter-firearm plots and their standard deviation ranges generally decrease as the sampling rate/bandwidth decreases, indicating that discrimination between the two sets (intra and inter) becomes greater.

FUTURE RESEARCH

As noted above, this research utilized high-quality recordings in a controlled environment; hence, conducting the same or similar research using recordings captured in non-anechoic but semi-controlled conditions (e.g., same microphone rig) and/or “real world” cases with known circumstances would likely shed more light on the results in conditions commonly encountered by forensic audio examiners. A simple, intra-firearm case example with known circumstances is presented in the Appendix.

Producing similar databases of controlled recordings using a wider array of firearms/ammunition would also improve the breadth of the data presently available and enable more detailed comparisons between firearm classes and specific models/ammunition.

The effects of bandwidth reduction on other quantitative measures, such as mean quadratic difference, and utilizing power data in lieu of waveforms in the same workflow could also be explored.

REFERENCES

1. Begault, D.R., S.D. Beck, and R.C. Maher, *Overview of Forensic Audio Gunshot Analysis Techniques*, in *2019 AES International Conference on Audio Forensics*. 2019: Porto, Portugal.

2. Maher, R.C., *Modeling and Signal Processing of Acoustic Gunshot Recordings*, in *2006 IEEE 12th Digital Signal Processing Workshop & 4th IEEE Signal Processing Education Workshop*. 2006. p. 257-261.

3. Maher, R.C., *Acoustical Characterization of Gunshots*, in *2007 IEEE Workshop on Signal Processing Applications for Public Security and Forensics*. 2007. p. 1-5.

4. Maher, R.C. and S.R. Shaw, *Deciphering Gunshot Recordings*, in *33rd International Conference: Audio Forensics*. 2008: Denver, USA.

5. The Mathworks Inc. *MATLAB R2019b "xcorr" function*. [cited 2019 November 6]; Available from: https://www.mathworks.com/help/matlab/ref/xcorr.html.

6. Lacey, D.S., B.E. Koenig, and C.E. Reimond, *The Effect of Sample Length on Cross-Correlation Comparisons of Recorded Gunshot Sounds*, in *54th International Conference: Audio Forensics*. 2014: London, UK.

7. Koenig, B.E., S.M. Hoffman, H. Nakasone, and S.D. Beck, *Signal Convolution of Recorded Free-Field Gunshot Sounds.* J. Audio Eng. Soc, 1998. **46**(7/8): p. 634-653.

8. Beck, S.D., H. Nakasone, and K.W. Marr, *Variations in recorded acoustic gunshot waveforms generated by small firearms.* J Acoust Soc Am, 2011. **129**(4): p. 1748-1759.

9. Maher, R.C. and E. Hoerr, *Forensic Comparison of Simultaneous Recordings of Gunshots at a Crime Scene*, in *147th Convention of the Audio Engineering Society*. 2019: New York, USA.

10. Maher, R.C. and T. Routh, *Advancing Forensic Analysis of Gunshot Acoustics*, in *139th Convention of the Audio Engineering Society*. 2015: New York, USA.

11. Maher, R.C., *Advancing Audio Forensics of Gunshot Acoustics*. 2018, National Criminal Justice Reference Service.

12. Maher, R.C. *Example recorded data*. 2018 [cited 2019 November 6]; Available from: http://www.montana.edu/rmaher/gunshots/gunshot_data.html.

13. Pohlmann, K.C., *Principles of digital audio*. 6th ed. 2011, New York: McGraw-Hill.

14. Koenig, B.E. and D.S. Lacey, *The Average Direct Current Offset Values for Small Digital Audio Recorders in an Acoustically Consistent Environment.* J Forensic Sci, 2014. **59**(4): p. 960-966.

15. Koenig, B.E., D.S. Lacey, C. Grigoras, S.G. Price, and J.M. Smith, *Evaluation of the Average DC Offset Values for Nine Small Digital Audio Recorders.* J Audio Eng Soc, 2013. **61**(6): p. 439-448.

16. The Mathworks Inc. *MATLAB R2019b "resamp" function*. [cited 2019 November 6]; Available from: https://www.mathworks.com/help/signal/ref/resample.html.

17. The Mathworks Inc. *Resampling*. [cited 2019 November 6]; Available from: https://www.mathworks.com/help/signal/ug/resampling.html.

18. Mendenhall, W. and T. Sincich, *Statistics for engineering and the sciences*. 5th ed. 2007, Upper Saddle River, New Jersey: Prentice Hall, Inc.

APPENDIX

Case Example

As a simple case example, fourteen (14) shots were fired from a handgun (Glock 22, .40 caliber) in an outdoor environment at night, near a microphone mounted within a law enforcement vehicle. The microphone signal was recorded onto one channel of the hi-fi stereo audio track of a VHS tape-based dashboard camera recording system. The individual firing the handgun was panning slightly from their left to right over the first ten (10) shots but was relatively still for the last four (4) shots, as observed in the video recording of a second dashboard camera recording system. Figure 29 displays the waveforms for these last four (4) recorded shots, as digitized at a sampling rate of 44.1 kHz from the VHS hi-fi audio track.

The methodology described in this thesis was applied to these last four (4) shots, each segmented into separate 175-millisecond WAV files, with the downsampling processes performed using the DC offset-corrected, 44.1 kHz digitized file segments. The results are provided in Table 9 and are displayed graphically in Figure 30. Additionally, the percent changes per kHz in the average maximum cross-correlation values are shown in Figure 31.

Table 9 – Average maximum cross-correlation values and their corresponding standard deviation values for the four (4) recorded gunshots in the case example for sampling rates 44.1, 32, 31.25, 24, 22.05, 16, 15.625, 12, 11.025, and 8 kHz.

Max CC value	Sampling Rate (kHz)									
	44.1	**32**	**31.25**	**24**	**22.05**	**16**	**15.625**	**12**	**11.025**	**8**
AVG	0.7175	0.7174	0.7176	0.7171	0.7176	0.7165	0.7165	0.7203	0.7191	0.7237
SD	0.1356	0.1356	0.1358	0.1355	0.1361	0.1345	0.1346	0.1366	0.1342	0.1346

From this case example, it is evident that bandwidth reduction had little impact on the average maximum cross-correlation values and corresponding standard deviations, but the results are generally consistent with those obtained from the controlled database recordings utilized in this research for the same 44.1 kHz to 8 kHz range (see Table 5 and Table 6 and the corresponding figures).

Both the average and standard deviation values from the case example were highly consistent across the sampling rates, with the overall average/standard deviation range being 0.7183±0.1353. The corresponding percent change per kHz results oscillated above and below 0%/kHz, with the values for the lowest sampling rate transitions (15.625 kHz/12 kHz, 12 kHz/11.025 kHz, and 11.025 kHz/8 kHz) having the greatest deviations.

As a general observation, the waveforms of the recorded gunshots in this case example (Figure 29) are noticeably different than those captured in the controlled database (as exemplified in Figure 9 through Figure 11). Whereas the controlled database recordings exhibit quick acoustic decay and return to the ambient noise level within approximately eleven (11) milliseconds, the recordings in the case example have much longer acoustic decay patterns and more complex signatures following the onset of the muzzle blasts. These differences are due in large part to the effects of the non-optimal microphone and recording system employed in the dashboard recording system.

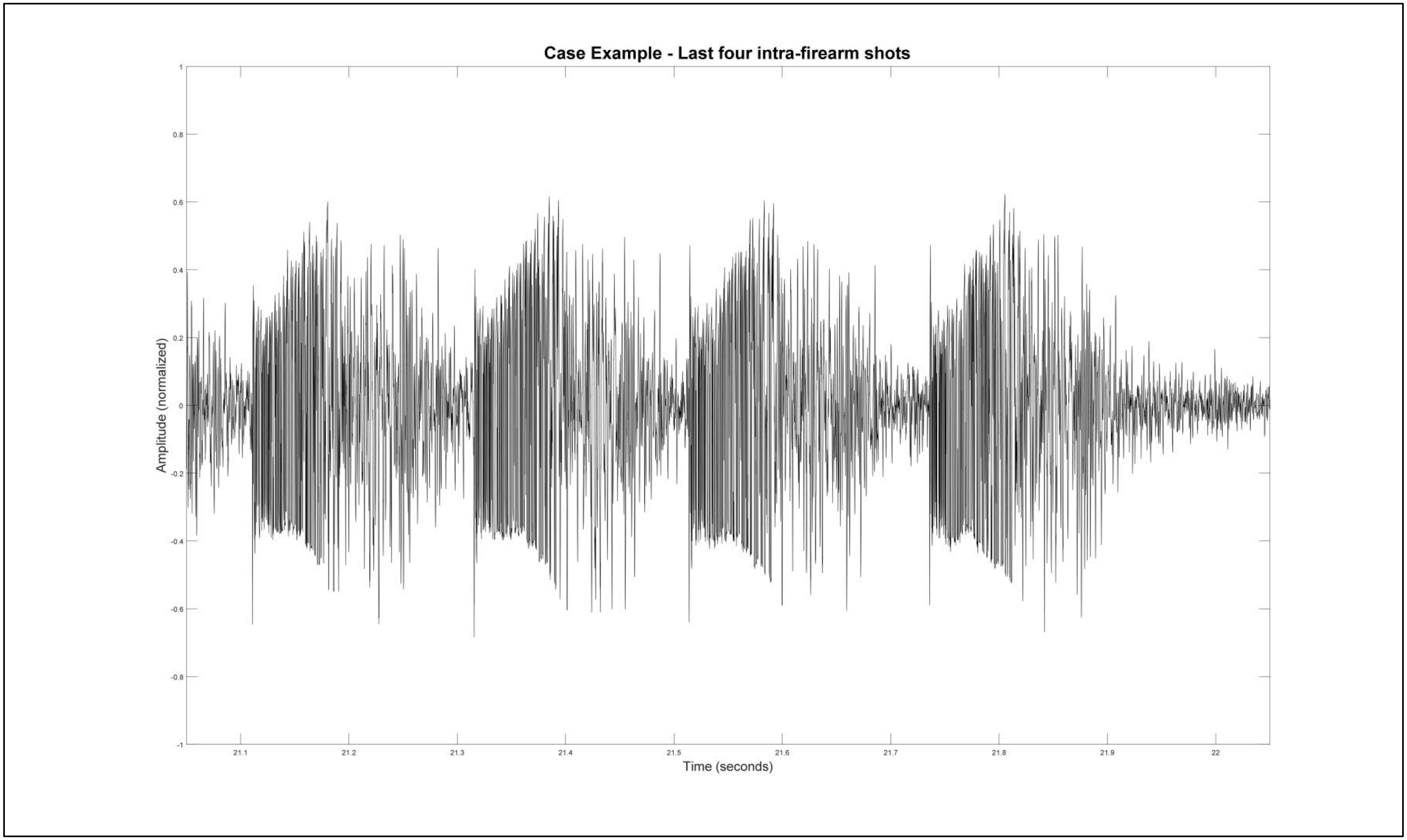

Figure 29 – Waveform display of the last four (4) recorded intra-firearm gunshots from the case example, over a one-second time span and with sampling rate of 44.1 kHz.

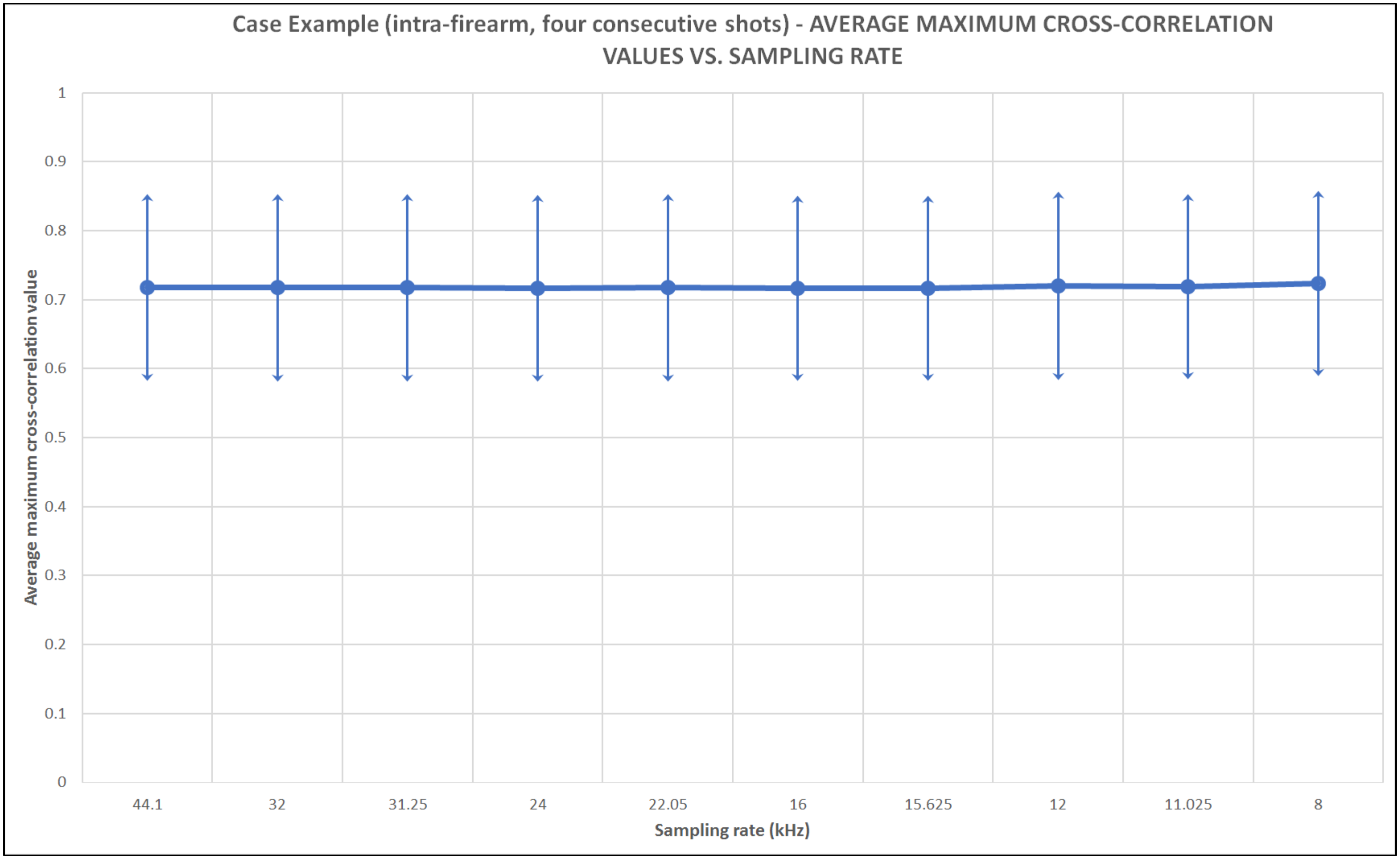

Figure 30 – Average maximum cross-correlation results vs. sampling rate for the last four (4) recorded gunshots in the case example. Standard deviation bars shown for each plot.

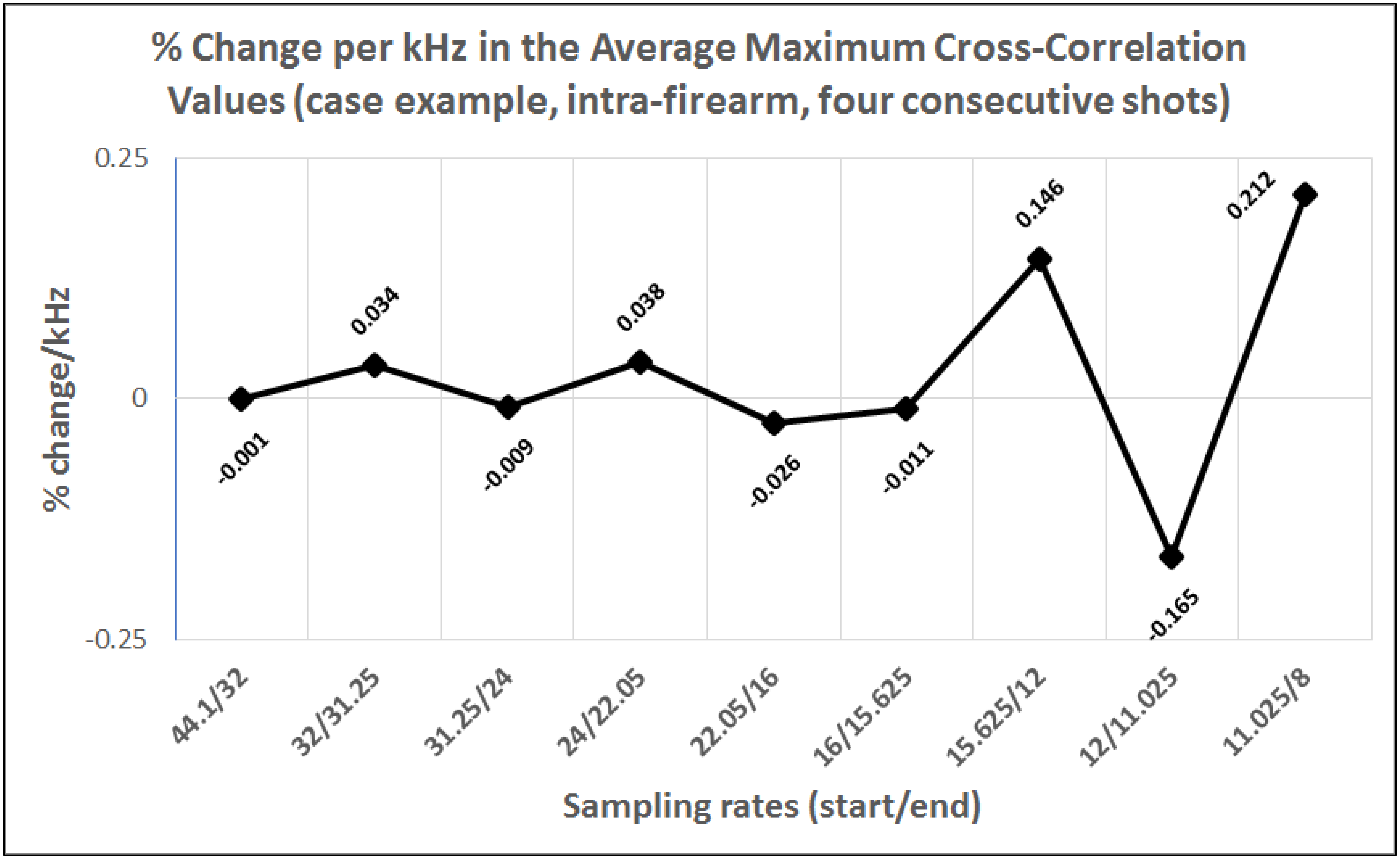

Figure 31 – Percent changes per kHz in the average maximum cross-correlation values for the four (4) recorded gunshots in the case example in successive sampling rate steps.